THE USE OF AN ULTRA-COMPACT COMBUSTOR AS AN INTER-TURBINE BURNER FOR IMPROVED ENGINE PERFORMANCE

THESIS

Jose L. Miranda Jr., Captain, USAF

AFIT-ENY-14-M-38

DEPARTMENT OF THE AIR FORCE
AIR UNIVERSITY

AIR FORCE INSTITUTE OF TECHNOLOGY

Wright-Patterson Air Force Base, Ohio

AFIT-ENY-14-M-38

THE USE OF AN ULTRA-COMPACT COMBUSTOR AS AN INTER-TURBINE
BURNER FOR IMPROVED ENGINE PERFORMANCE

THESIS

Presented to the Faculty

Department of Aeronautical and Astronautical Engineering

Graduate School of Engineering and Management

Air Force Institute of Technology

Air University

Air Education and Training Command

in Partial Fulfillment of the Requirements for the

Degree of Master of Science in Aeronautical Engineering

Jose L. Miranda Jr., B.S.M.E.

Captain, USAF

March 2014

AFIT-ENY-14-M-38

THE USE OF AN ULTRA-COMPACT COMBUSTOR AS AN INTER-TURBINE

BURNER FOR IMPROVED ENGINE PERFORMANCE

Jose L. Miranda Jr., B.S.M.E.
Captain, USAF

Approved:

//signed//	14 Mar 2014
Marc D. Polanka, PhD (Chairman)	Date
//signed//	14 Mar 2014
Lt Col Anthony M. Deluca, PhD (Member)	Date
//signed//	14 Mar 2014
Lt Col Ronald J. Simmons, PhD (Member)	Date

AFIT-ENY-14-M-38

Abstract

An Inter-Turbine Burner (ITB) represents a novel mechanism for generating additional work from a gas turbine engine in applications where an afterburner would typically be used. An ITB can achieve higher thermal efficiencies over a typical afterburner while also generating shaft work versus only additional thrust.

In an effort to investigate the potential applications for the ITB, a numerical engine cycle comparison was made between the ITB cycle and a conventional afterburning cycle using the Numerical Propulsion System Simulation (NPSS). In the case of thrust augmentation, the ITB model outperformed the afterburning model when Thrust Specific Fuel Consumption (TSFC) is compared to increased thrust, but resulted in decreased fan efficiency and High Pressure Compressor (HPC) stall caused by fan overspeed. In the case of Power Extraction (PX) augmentation the ITB engine achieves similar TSFC results without experiencing component efficiency loss or approaching HPC stall. For the PX augmentation model, the pressure drop across the ITB was varied from 4% to 20%. Large pressure drops were found to increase the TSFC and reduce the HPC stall margin for the ITB model. ITBs are expected to achieve pressure drops between 3% and 5% and for this range the ITB will continue to be more fuel efficient than the afterburning engine model.

An experimental investigation was performed focused on integrating the Air Force Institute of Technology (AFIT) ITB to accept a common flow source. Three common flow source diffusers with core to bypass inlet area percentage ratios of 80/20, 70/30, and 60/40 were tested. All three diffuser designs were found to suffer from flow reversal in the bypass stream caused by instances of greater total pressure in the core flow than in the bypass flow. The baseline thrust performance for the JetCat P200 Small Turbine Engine (STE), which will serve as the AFIT ITB vitiated air source, was determined and found to be consistent with manufacturer specifications.

iv

Table of Contents

List of Figures

Figure   Page

List of Tables

List of Symbols

Symbol   Definition

P	pressure (kPa)
T	temperature (K)
V	velocity (m/s)
dP/qP	pressure drop
R_{mix}	mixer total pressure ratio
ϕ	equivalence ratio

Subscripts

t	total
s	static

List of Acronyms

Acronym	Definition
AB	Afterburner
AFIT	Air Force Institute of Technology
AFRL	Air Force Research Laboratory
BPR	Bypass Ratio
CFD	Computational Fluid Dynamics
COAL	Combustion Optimization and Laser
ECU	Engine Control Unit
EV	EnVironmental
FPR	Fan Pressure Ratio
GE	General Electric
GSU	Ground Support Unit
HP	High Pressure
HPC	High Pressure Compressor
HPT	High Pressure Turbine
HRR	Heat Release Rate
ISSI	Innovative Scientific Solutions Incorporated
ITB	Inter-Turbine Burner
JSF	Joint Strike Fighter
LBO	Lean Blow Out
LDV	Laser Doppler Velocimetry
LLCB	Low Loss Center Body
LLP	Longwell Loading Parameter
LP	Low Pressure

Acronym	Definition
LPT	Low Pressure Turbine
MD	Middle Diameter
NASA	National Air and Space Administration
NPSS	Numerical Propulsion System Simulation
OD	Outer Diameter
OFAR	Overall Fuel/Air Ratio
OPR	Overall Pressure Ratio
POI	Point of Interest
PR	Pressure Ratio
PW	Pratt and Whitney
PX	Power Extraction
SC	Sequential Combustion
SCC	Sequential Combustion Cycle
SEV	Sequential EnVironmental
ST	Specific Thrust
STE	Small Turbine Engine
T-s	Temperature and Enthalpy
TIT	Turbine Inlet Temperature
TSFC	Thrust Specific Fuel Consumption
TVC	Trapped Vortex Combustor
UAS	Unmanned Aircraft System
UCC	Ultra-Compact Combustor
VABI	Variable Area Bypass Injector
VCE	Variable Cycle Engine
VI	Virtual Instrument

THE USE OF AN ULTRA-COMPACT COMBUSTOR AS AN INTER-TURBINE

BURNER FOR IMPROVED ENGINE PERFORMANCE

I.   Introduction

The constant demand for high performance gas turbine engines has lead researchers to investigate novel approaches for new engine designs. Ideally, designers would like to produce an engine with a high thrust-to-weight ratio and reduced fuel consumption. Shortening the combustion section of a gas turbine engine reduces the total weight of the engine, but significant problems arise including reduced residence time in the combustor, i.e., the time allowed for combustion to complete in the combustor. This reduced residence time leads to problems such as degraded engine efficiency, and the potential for fuel rich core air flow into the turbine section. The Air Force Institute of Technology (AFIT) has been investigating the use of an Ultra-Compact Combustor (UCC) to solve the residence time problem for a shortened combustion section by allowing the air flow in the combustion section to travel in a circumferential direction; therefore, completing combustion before the core flow enters the turbine section. This shortened combustion section is being considered for the potential application as an Inter-Turbine Burner (ITB). An ITB reheats the flow leaving the first turbine stage to enable more work to be extracted from the cycle in the following turbine stage. This work can be used for either additional thrust, as a typical afterburner, or to generate additional shaft power. This power could then be intermittently modulated and applied during higher demand periods such as takeoff or to power needed electrical systems [1].

1

Ultra-Compact Combustor

The UCC concept is an approach to shortening the axial length of an engine while still providing adequate residence time in the combustor to achieve complete and efficient combustion. The UCC concept used in place of a conventional combustor can be seen in Figure 1. Significant research has already been performed in the area of UCC development; and UCCs have been shown to provide improved combustion efficiency over conventional annular combustors. The AFIT UCC uses circumferential high *g* combustion to provide the residence time required within a significantly shortened axial length. With the development of UCC technology, the aerospace industry can consider reheat cycles which capitalize on the reduced size and weight of a UCC.
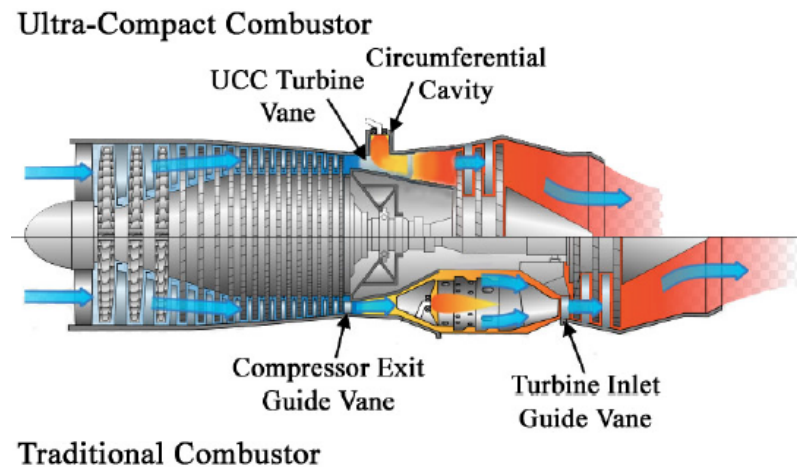
Figure 1: UCC and Traditional Combustor Systems Comparison [2]

Inter-Turbine Burning

Conventional multistage turbine engines are disadvantaged by the temperature loss that occurs between the turbine stages. The reduced fluid temperature experienced by each additional turbine stage limits the work that can be extracted for each stage. This same problem has been recognized and addressed in the power generation industry utilizing

continuous reheat gas turbines which ideally operate on the Continuous Temperature (CT) cycle. A CT cycle has greater efficiency and reduced fuel consumption than the Brayton cycle used by most gas turbines for aeronautical applications [3].

An ITB is a form of a second stage combustor differing from an afterburner in that more work can be extracted from the heat addition. The additional shaft power provided by the heat addition from the ITB could be used to augment increased power requirements, and may be more desirable than a traditional afterburner for select mission types and requirements. The ITB can be used to increase the amount of work performed by an engine cycle without raising the maximum cycle temperature. If the temperature entering the Low Pressure Turbine (LPT) is raised to the same temperature entering the High Pressure Turbine (HPT), then a typical cooling scheme used on HPT turbines could be used on the LPT turbine as well to handle the increase in temperature.

Research Objectives

The objective of this work is to investigate the instances in which an ITB engine cycle is more beneficial, in terms of fuel efficiency, than a conventional afterburning engine cycle, and to make progress towards integrating the AFIT UCC to function as an ITB. Studies concentrating on the benefits and consequences of incorporating an ITB into a practical engine design need to be conducted. This will allow engine designers to take advantage of the ITB concept as the technology matures. To address this need, a numerical analysis comparing an ITB engine cycle to a conventional afterburing cycle was conducted to establish circumstances where the ITB cycle is more beneficial. Numerical modeling can be used to determine the design parameters the ITB must achieve in order to outperform a conventional afterburner. To this extent a pressure drop study was accomplished to determine the range of pressure drop values the ITB must not exceed to provide more fuel efficient performance than an afterburner.

The ITB is conceptually beneficial to an engine cycle, but has yet to be fully integrated into a full scale engine. ITBs must be significantly smaller than conventional annular combustors to be used in a practical engine application. Current UCC technology uses high-g combustion to reduce the size of a conventional combustor by up to 66% [4]. The UCC allows for combustion to complete in the circumferential direction within UCC, as opposed to the axial direction as in a conventional annular combustor. This shortened combustor can be considered for integration into an ITB configuration. Currently, most ITB research employs a separate air stream, much like a traditional engine bypass duct, to provide the circumferential flow in an ITB cavity. The AFIT ITB provides air mass flow to the circumferential cavity using only a single core flow source. To accomplish this a diffuser design that divides the incoming air flow into a core and bypass stream was tested.

II. Background

UCC research has been conducted by various agencies to include the Air Force

Research Laboratory (AFRL) and AFIT. The main emphasis of this research has been to

reduce the size of a gas turbine engine combustion section while achieving improved

engine performance. This work has also been extended to include research into the use of

a UCC as an ITB. The research literature on these topics provides a basis of knowledge

from which to expand the field of study. This chapter explores the research done in the

past to lead to a better understanding of the topic. The knowledge to accomplish the

objectives established for this work was gained from an understanding of the volume of

work previously accomplished.

Ultra-Compact Combustor

The development of a UCC seeks to exploit physical phenomena, such as g-loading,

that can significantly reduce the time required to complete combustion in a gas turbine

engine's combustion section. Lewis discovered one such physical phenomena, buoyant

bubble transport, that has become the basis for UCC design. While studying the effects of

centrifugal force on combustion, Lewis noted at high values of centrifugal force, the flame

speed was greater than the predicted turbulent flame speed. His research used a

combustion centrifuge as depicted in Figure 2. The combustion centrifuge was charged

with a combustable mixture of either propane-air or hydrogen-air, and then rotated to the

desired speed before combustion was initiated. The data collected from these experiments

show for centrifugal force values below 200 g, flame propagation rates were unaffected.

Once the centrifugal force reached 500 g, the flame propagation rate increased with

increasing centrifugal force. This trend continued until a force of 3500 g, when the flame

propagation rate abruptly began to decrease. Lewis' work determined that fire will spread

at the fastest of the three flame propagation rates, which consist of laminar flame transport, turbulent flame transport, and buoyant bubble transport [5].
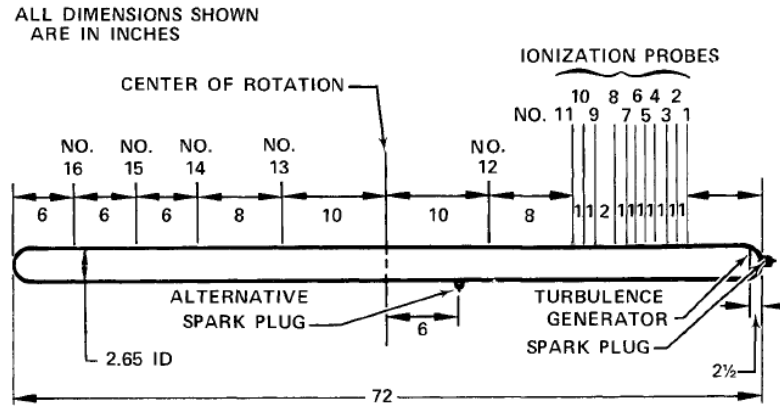
Figure 2: Combustion Centrifuge [5]

Zelina et al. [6] used the Anthenien UCC [7] to numerically confirm the bubble transport phenomena. A first order numerical analysis was conducted on a tube similar to that in the Lewis experiment, and used hydrogen-air mixture with an equivalence ratio of 0.8. Figure 3 show the results obtained from the 10g and 500g cases. For the 10g case, the flat flame front propagated at a velocity of ~1.86 m/s, which is close to the laminar flame speed at the reference condition. For the 500g case, the flame structure changes significantly, creating a mushroom vortex and propagating at a flame speed of 9.2 m/s, confirming the bubble transport theorem proposed by Lewis.

Yonezawa et al. built and tested a jet swirl combustor using the knowledge gained from the Lewis experiment. The goal of this research was to find a means by to increase the combustor loading in a gas turbine engine; and therefore, reduce the combustor length and maintain or improve combustion efficiency. The combustor design looks much like a traditional annular combustor with air injection ports that were capable of driving the flow circumferentially. By swirling the flow within the combustor liner they were able to achieve g-loads high enough to enhance mixing, and reduce residence time by taking

6

(a) 10g   (b) 500g
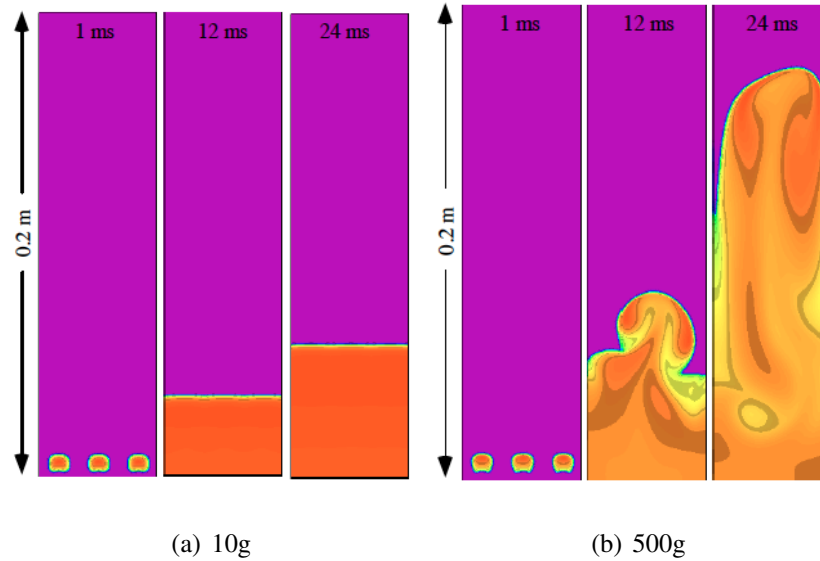
Figure 3: Spreading Flame Under G-loading [6]

advantage of buoyancy bubble transport. The jet swirl combustor was capable of achieving efficiencies of 99.5% with a combustor length 33% shorter than a conventional combustor [8].

Research in the use of swirling flow to reduce the size of gas turbine engine combustors has been extended well past the jet swirl combustor. AFRL has spent considerable time exploring the concept of a UCC that takes advantage of the use of high g combustion. Anthenien et al. constructed a small scale, atmospheric pressure laboratory combustor, with a circumferential cavity, that uses high g swirled flow for flame stabilization [7]. The combustor was instrumented, and tests were conducted with ethanol and JP-8 fuels. This combustor design seeks to burn rich in the circumferential direction before burning lean in the main flow, thereby significantly shortening the combustor. In order to impart a counterclockwise swirl within the combustor air could be introduced through the circumference at an angle of 45°, or through the fore and aft walls of the combustor at an angle of 15°. The air introduction can be seen in Figures 4(a), 4(b), and

4(c). Various parameters were varied in studying the operating range of the combustor. These parameters consisted of main airflow, ring airflow, plate airflow and fuel flow.
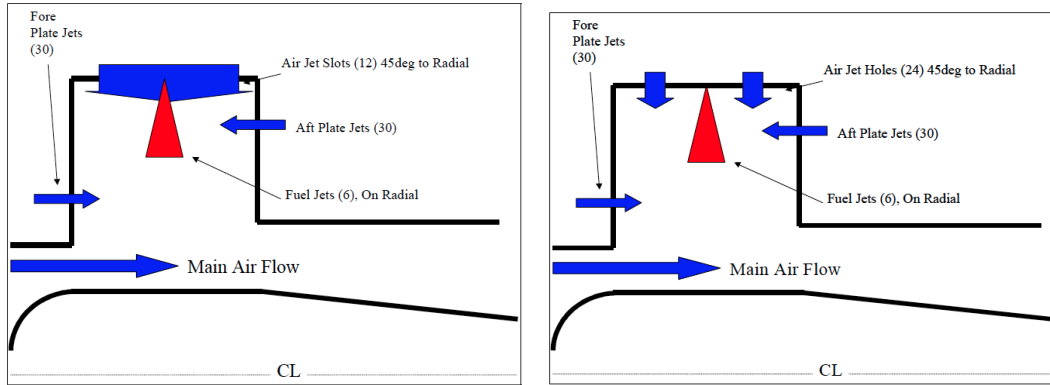
(a) Illustration of Jet Slot Design

(b) Illustration of Straddle Jet Design
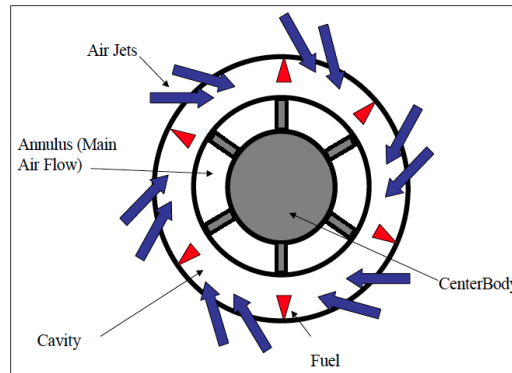
(c) Illustration of Circumferential Air Introduction

Figure 4: Air Introduction for the Anthenien UCC [7]

Two designs were tested for the introduction of air through the circumference of the combustor. In the first design iteration, see Figure 4(a), air was introduced through twelve slots. This design produced poor results with low efficiencies and poor ignition characteristics. The poor performance of this design was attributed to the curtain of air from the slot collapsing the fuel spray and degrading the fuel/air mixing. The combustor was run using only air introduced through the fore and aft walls. This method also performed poorly and only yielded efficiencies of 80% to 92%. The second design

iteration, see Figure 4(b), matched the area of the twelve slots used in the first design, but the single slots were replaced with twelve pairs of round holes that introduced air on either side of the fuel spray. This "straddle jet" design yielded significantly better results. The equivalence ratio, ϕ, in the circumferential cavity was well within the rich region with a $\phi = 1.6$, and a very short flame. The combustor was capable of producing efficiencies greater than 99% using both ethanol and JP-8 fuels. Also noted was as the loading in the cavity increased so did the efficiency, which is the opposite trend of a conventional combustor. The increased efficiency was attributed to a g-loading increase as the air mass flow into the cavity increased. Increasing efficiency could only be achieved up to the point where the cavity loading, and therefore g-loading, decreased the residence time in the cavity to a point at which blow out would occur. The effects of cavity loading can be seen in Figure 5, which shows that the UCC is capable of decreasing the Longwell Loading Parameter (LLP) (increased air loading) by almost and order of magnitude over conventional combustors. The LLP is used to normalize the size and pressure effects of different combustors at different operating conditions, and is calculated using Equation 1 [9].

$$LLP = \frac{VP^{1.75}e^{\frac{T}{300}}}{\dot{m}}$$

(1)

Quaale et al. [9] conducted Laser Doppler Velocimetry (LDV) within the circumferential cavity of the Anthenien UCC. For these experiments the air was swirled in the cavity using the "straddle jet" configuration in Figure 4(b). Data was collected over a 60° segment of the UCC, which contained a fuel injector and 4 pairs of air injection holes spaced 20° apart. Velocity measurements were taken within the cavity at three locations, 16° downstream of the fuel injector, and 4° upstream of a pair of air injection holes. The measurement positions can be seen in Figure 6. Positions A and C are in the air injection jet plane, and position B is in the fuel injection plane.

9
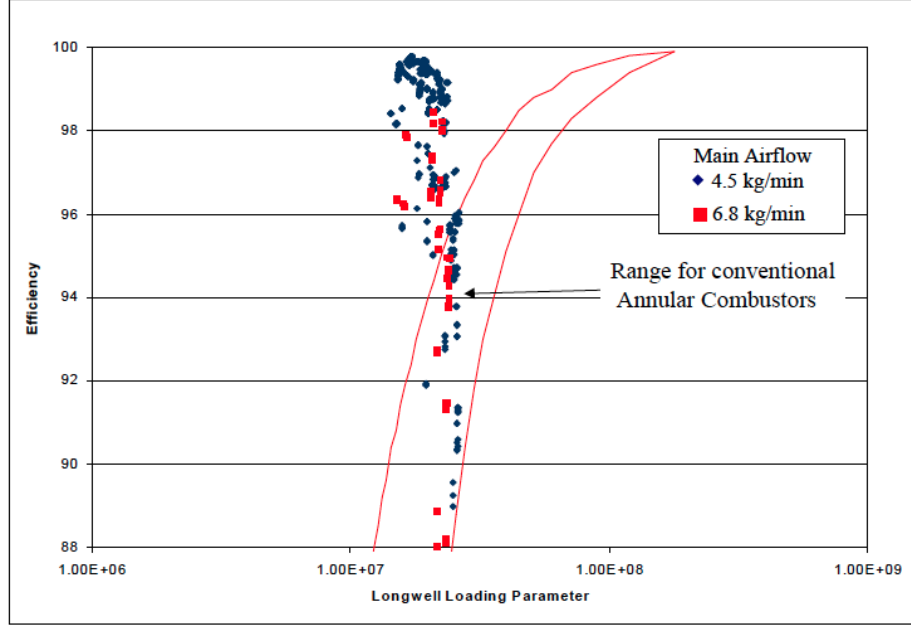
Figure 5: Efficiency vs. LLP for Varied Main Airflow Rates [7]

Data was taken for equivalence ratios from 0.8 to 1.5, and the cavity velocity was insensitive to variation in equivalence ratio. In the air jet plane, circumferential velocities ranged form 20 to 45 m/s with radial velocities ranging from 2 to 12 m/s, with 22% of total air flow through the cavity. The air jet plane data was collected at stoichiometric conditions, and the pressure drop across the combustor was varied from 1% to 4%. From the measurements taken, the cavity g-loading dependance on air mass flow is illustrated for position A in Figure 7. The cavity g-loading was calculated with Equation 2.

$$g = \frac{U_\theta^2}{g_o R} \qquad (2)$$

Velocity measurements were taken in plane with the fuel injector with 22% of the total air flow through the cavity at stoichiometric conditions. Circumferential velocities were measured between 20 to 30 m/s with tangential velocities ranging from 7 to 10 m/s. The velocities, as expected, were lower in the fuel injection plane as compared to the air

10
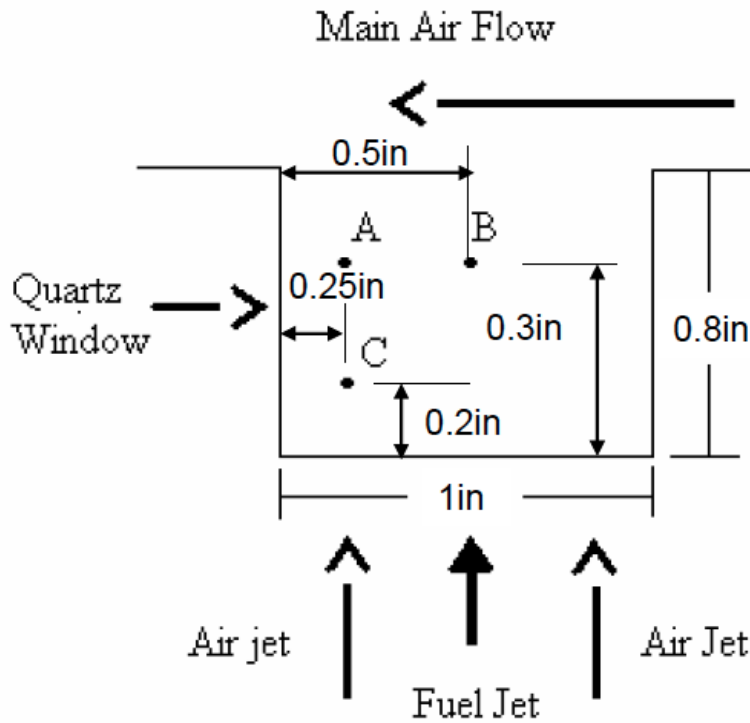
Figure 6: Diagram of LDV Measurement Positions A, B and C [9]

injection plane. A Computational Fluid Dynamics (CFD) analysis was performed using a 60° wedge that contained the four air injection locations and the single fuel injector with a 4% and a 2% pressure drop. Results from the CFD study compared well with the experimental results at the same conditions. The CFD study also showed a strong temperature stratification in the radial direction of the cavity. This is the result of g-loading forcing the cooler, denser fluid against the outer circumference of the cavity, while the lighter combustion products migrate toward the inner circumference. This contributes to shorter residence times and high efficiencies experience by the UCC. The LLP was used to compare the efficiencies of conventional combustors to the UCC. The same trend identified by Anthenien was also noted that as the LLP increases the UCC efficiency decreases, which is the opposite trend as conventional combustors.
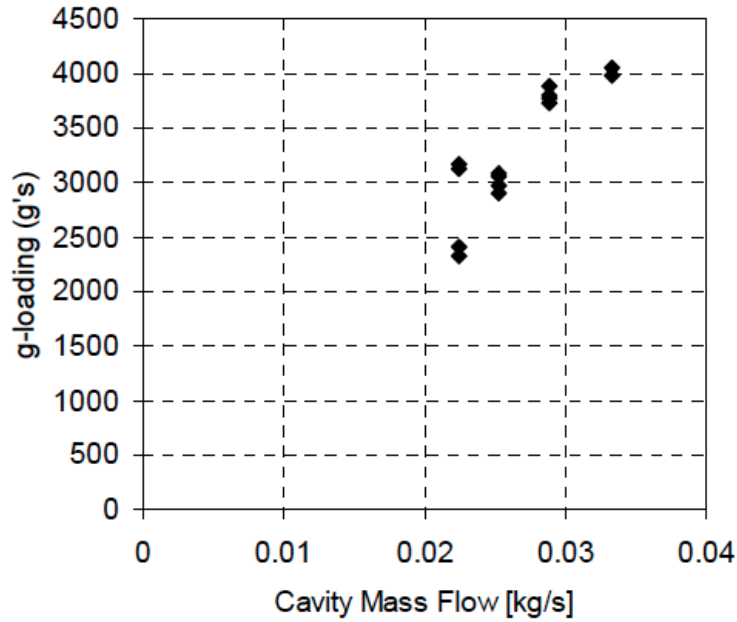
Figure 7: G-loading vs. Cavity Mass Flow at Stoichiometric in the Cavity (Position A) [9]

Zelina et al. [6] studied the Heat Release Rate (HRR) in the circumferential cavity of the Anthenien UCC. The UCC was tested with a 22% air mass flow split into the cavity with pressure drops varying from 2% to 5%, and cavity equivalence ratios from 0.75 to 2.2. Figure 8 show the data collected for the temperature rise in the cavity versus the HRR and the pressure drop in the cavity. The HRR was found to be a strong function of pressure drop which suggests that for a given HRR, the cavity volume can be reduced while maintaing a constant temperature if the pressure drop is increased.

The operability of the UCC was investigated and it was found that the Lean Blow Out (LBO) was much lower than that of a conventional combustor. The data showed that the UCC could operate at three times the air loading parameter (inverse of LLP) of a conventional system. Figure 9 shows the LBO performance of the UCC, and suggests the UCC can maintain a flame up to a g-loading of 7000g to 8000g. This data corresponds well with the data from the Lewis experiment, which showed that a flame will extinguish at ~8000 g's.
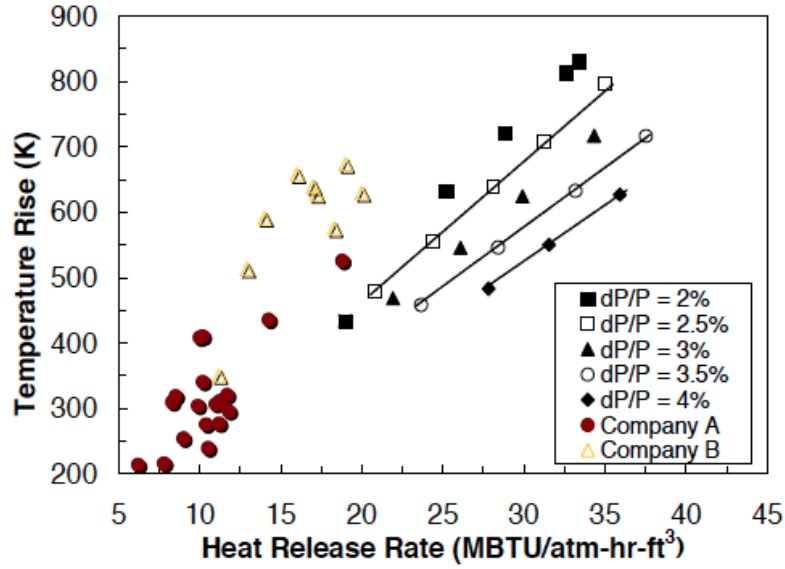
Figure 8: HRR for UCC Compared to Conventional Combustor Primary Zone Values [6]
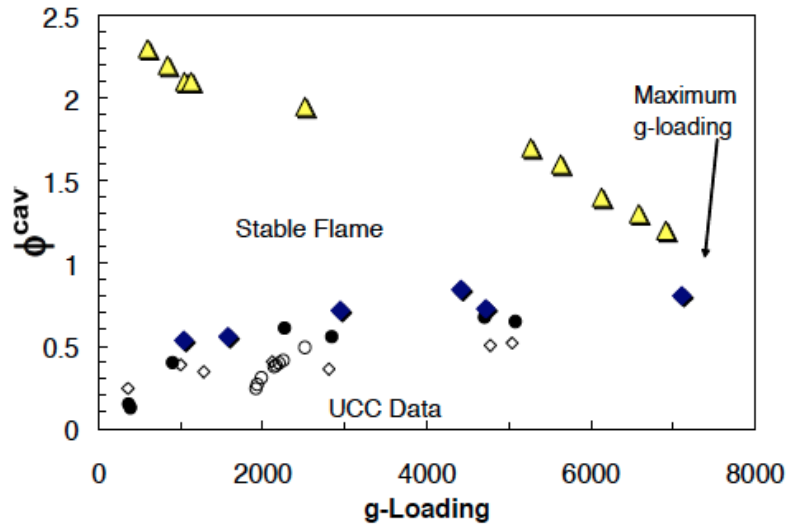
Figure 9: UCC Cavity Equivalence Ratio at Blowout as a Function of Cavity G-loading [6]

Their research also noted a possible combustion efficiency dependance on liquid fuel atomization. The data showed when fuel atomization provides droplets ~20 μm, the flame speed is dictated only by the g-loading and the cavity reaction temperature. The flame speed was calculated using Equation 3 where S_b is the burning velocity, T_u is the inlet air

temperature, T_b is the calculated adiabatic flame temperature of JP-8/air, and g is the cavity g-loading. The data for combustion efficiency versus cavity reaction temperature and g-loading can be seen in Figure 10. The work done by Zelina et al. [6] demonstrated the UCC is capable of combustion efficiencies greater than 99%, with flame lengths 50% shorter, and twice the HRR than that of convention combustors.

$$S_b \propto \frac{T_b}{T_u} \sqrt{g} \tag{3}$$
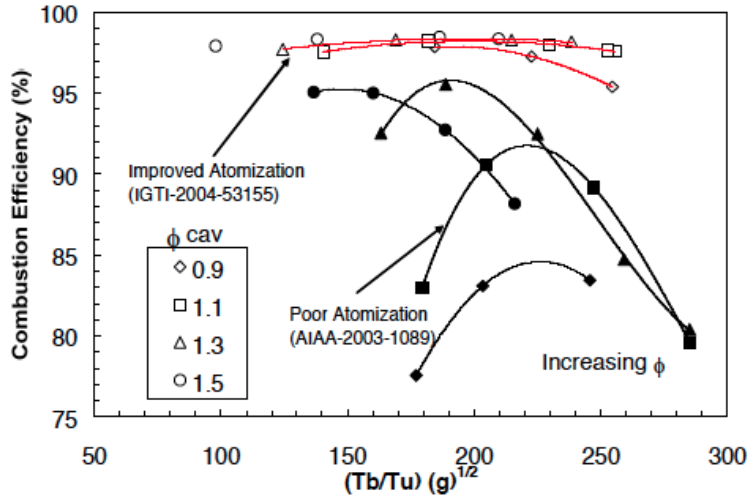
Figure 10: Effects of Atomization Quality on the Correlation Parameter for High G Combustion [6]

AFRL has also developed a different method to approach the use of high g combustion in a UCC. Blunck et al. [10] studied a UCC that swirls the flow in the cavity in a direction tangent to the circumference of the combustor, which is referred to as a Trapped Vortex Combustor (TVC). A diagram of the TVC is shown in Figure 11.

Blunk et al. [10] performed a cycle analysis to determine the potential benefits of using a UCC as a main combustor. Their data showed for a 4% improvement in pressure ratio across the UCC, a 1% improvement in Thrust Specific Fuel Consumption (TSFC)
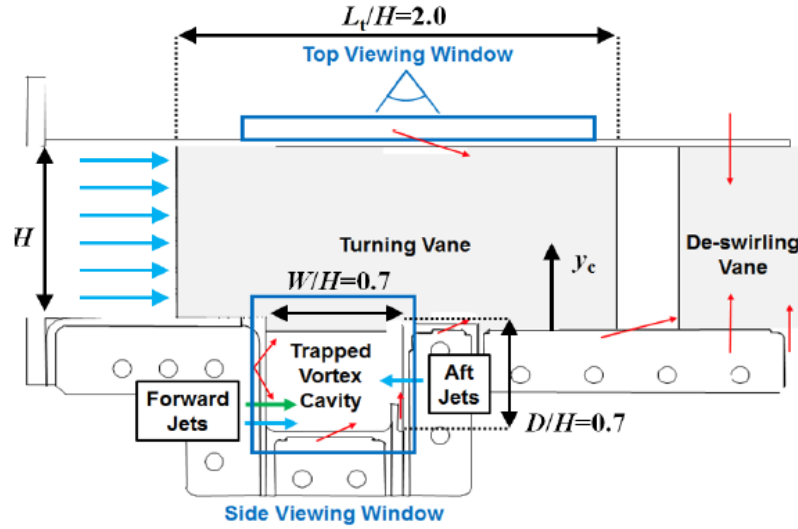
Figure 11: Illustration of Side View of Combustor where Air Driver Jets and Inlets are Shown in Blue, Fuel Injectors in Green, and Effusion Cooling in Red [10]

was achieved, as seen in Figure 12. Combustor length and weight calculations were also performed, and they determined every 2.5 cm reduction in combustor length resulted in a 0.4% reduction in engine weight. By eliminating the last stage compressor stator and the first stage turbine vane by combining and incorporating them into the TVC, a length savings of ~30% resulted. This reduction in engine length translates into a 2.4% savings in total engine weight.

Physical testing of the UCC was conducted using a planar section of the TVC concept. The sectional UCC allowed for the investigation of combustion efficiency, NO_x emissions, profile factor, and fluid mechanics within the cavity for various combustor configurations and mass flows. Their work found increasing the air loading (inverse of LLP) in the cavity allows for additional chemical energy to be released. Combustion efficiencies greater than 99% were observed for combustor configurations yielding the highest vortex strengths. This effect is only beneficial to the point where excessive air loading leads to poor flame stability, reduced combustion efficiencies, and poor emissions profiles caused by high flame shear rates. It was also observed that stronger vortical
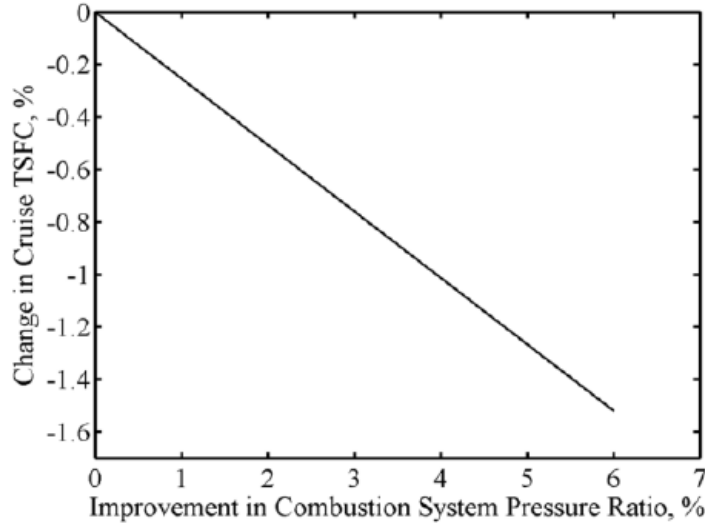
Figure 12: Change in TSFC for Improvements in Combustion System PR for Commercial-Class Engine Operating at M = 0.8 [10]

structures improved combustion efficiencies by enhancing mixing and reducing residence time for the completion of reactions. The data can be seen in Figure 13 for varied combustor configurations.
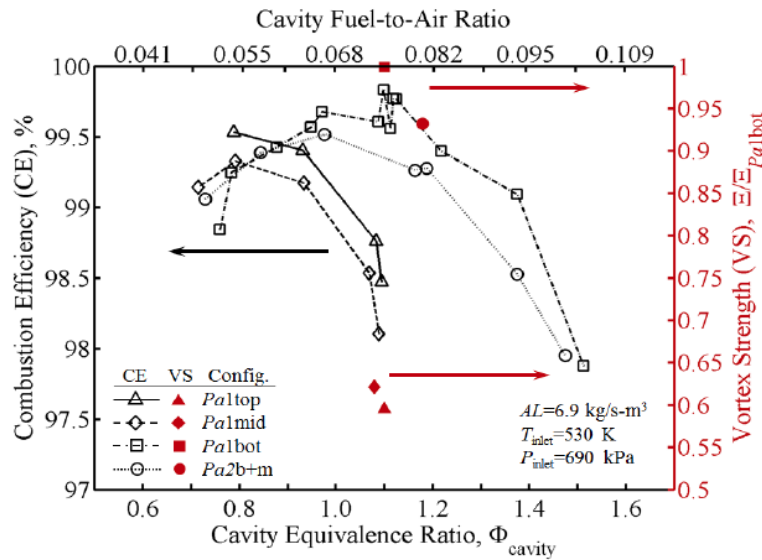
Figure 13: Combustion Efficiency and Normalized Vortex Strength as Function of Cavity ϕ [10]

The most recent work conducted in the AFIT Combustion Optimization and Laser (COAL) lab is that of Wilson et al. [11] This research uses a UCC similar to that of the Antheinian UCC, but is larger and provides greater optical access. The AFIT UCC is ~16 cm in diameter with a cross sectional area of 6.5 cm². It utilizes the the Anthenien straddle jet design with 24 paired holes angled at 35° tangent to the circumference to create the cavity swirl. The UCC can be run on either propane or JP-8. The objectives of the work was to study the lean blow out limits of the UCC, the impact of air injection hole diameter, the effects of swirl direction in the cavity, and the g-loading effects on the atomization, mixing, and ignition of liquid fuels. Figure 14 shows a cut away view of the AFIT UCC.
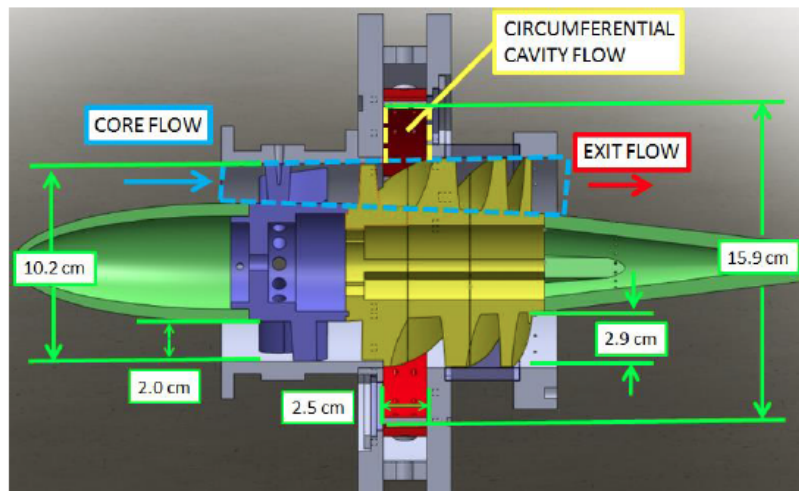
Figure 14: AFIT Full Annulus UCC [11]

Lean blowout performance of the AFIT UCC was consistent with that of Zelina et al. [6] in that as the g-load in the cavity increased a high cavity equivalence ratio was required to sustain a flame within the UCC cavity. They also noted operating above lean blowout does not ensure uniform cavity characteristics as an instability region prior to lean blowout was observed. The air injection hole diameter had a significant effect on cavity g-loading.

The g-loading was found to decrease as the hole diameter increased. A hole diameter of 0.45 cm was found to yield the best results when g-loading and flame stability were considered. The impact of swirl direction showed clockwise swirl direction is preferred. The counterclockwise swirl direction suffered from flame unsteadiness attributed to the flow turning ~135° before exiting the cavity. Fuel spray testing under g-loading showed as g-loading increased the penetration depth of the fuel was reduced, thereby keeping the fuel in the cavity longer, which allows combustion reactions to complete within the cavity.

Inter-Turbine Burning

The UCC reduces the size and weight of a gas turbine engine's main combustor. With the potential for shortened combustors on the horizon, it has been proposed that sequential combustion, or inter-turbine burning, can be allied to the aerospace industry to achieve improved engine performance. Research is ongoing at AFIT and AFRL in the area of applying the UCC as an ITB.

Sequential Combustion (SC) is not a new concept to gas turbine engines. Alstom, formally known as ABB Power Generation, developed a line of SCgas turbines for the power generation industry [12]. The Alstom GT24 and GT26 consist of a primary combustor a turbine and a reheat combustor, with the aim of achieving high efficiency while delivering low emissions. Alstom has been utilizing the SC concepts since the 1940's using diffusion type combustors. In 1995 Alstom developed their modern line SC gas turbines shown in Figure 15. The GT24/GT26 uses an EnVironmental (EV) main combustor followed by a single stage turbine. After the first turbine, a Sequential EnVironmental (SEV) combustor is used to reheat the fluid before expanding it through a four stage second turbine. Both combustors are operated at low loads of ~10-25%, and at full load both combustors have approximately equal fuel flows.
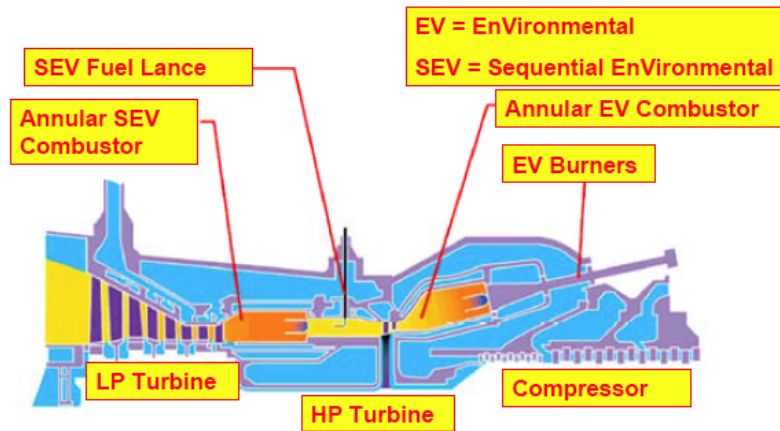
Figure 15: GT24/GT26 Cross Section [12]

With the successful use of SC in the power generation, Vogeler proposed the Sequential Combustion Cycle (SCC) for use in aircraft engines [13]. For a conventional turbofan with a single combustor, thrust is a function of bypass ratio and maximum pressure and temperature in the cycle. Considering a twin spool turbofan engine as reference, if inlet mass flow is kept constant, increasing the bypass ratio reduces the mass flow through the core. The reduced core mass flow limits the fuel flow that can be feed to the combustor limiting, the potential energy extracted by the engine. With the use of a SCC, an engine designer has another parameter to vary for improving engine performance. The purpose of the Vogeler study was to compare the use of a conventional single combustor turbofan cycle to a turbofan utilizing the SCC. The study revealed a dual spool turbofan may actually suffer from the use of SCC. This is due to the fact the reduced fuel flow into the first combustor means there may not be enough energy available to the second combustor to build enough pressure for an economical second expansion in the low pressure turbine. The SCC engine with a single shaft delivered 24% higher Specific Thrust (ST) than a conventional engine with a hot gas temperature of 1740 K. The most significant benefit of the SCC is more energy can be introduced to the cycle without raising the maximum cycle temperature.

Liu and Sirignano [14] investigated an engine cycle using the ITB in a turbojet and turbofan engine to improve engine performance. They determined the use of an ITB for engine augmentation would reduce the afterburner length and width, reduce specific fuel consumption, and increase specific trust compared to an afterburning engine. Ideally, it is more desirable to burn at constant temperature in the turbine rotor, but this can prove difficult. The ITB avoids the problems associated with burning in the turbine rotor by burning between turbine stages, and can potentially be combined with the turbine stators to reduce the length of the ITB. Figure 16 shows Temperature and Enthalpy (T-s) diagrams for the ideal turbine burning cycle compared to potential ITB cycles.
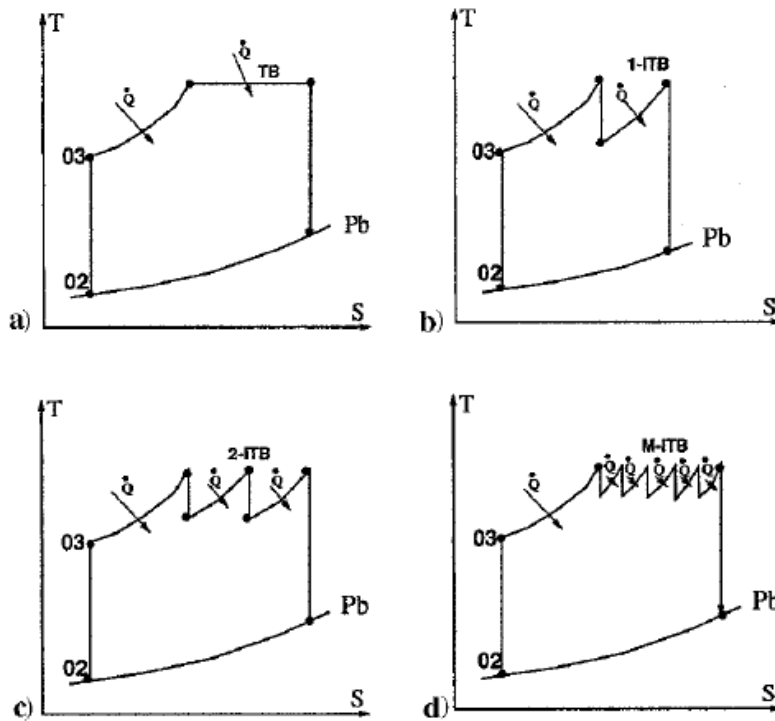
Figure 16: Turbine Burning and ITB Cycles [14]

Lui and Sirignano's [14] research into the ITB cycle determined turbine burning engines benefit from higher compressor pressure ratios. While conventional engines have

optimal compressor pressure ratios between 30 to 40, the ITB cycle can operate at compressor pressure ratios higher than 60. High compression ratios translate to increased ST, and reduced TSFC. The ITB cycle was found to be superior to conventional engines at high flight speeds. ITB engines should be designed to achieve an optimal power distribution across the turbines for a given mission or engine configuration. By designing to the optimal power distribution the best thermal efficiency of the ITB cycle can be achieved. With careful design considerations a single ITB turbofan engine provides more than 50% greater ST, with an equal TSFC as a conventional turbofan engine.

Liew et al. [15] conducted a performance cycle analysis of a dual spool turbofan with separate exhaust using an ITB as the second combustor. Figure 17 shows the T-s diagram for the engine cycle investigated. Performance cycle analysis is also known as off-design analysis, which is used to determine the performance of a reference engine operating at conditions other than those for which it was designed. Two engines were studied, engine A is a low bypass turbofan with a Bypass Ratio (BPR) of 0.73 and engine B is a high bypass turbofan with a BPR of 4.0. These engines are compared to un-augmented variants for the same engine. Full and partial throttle operations were studied. For full throttle operation both the main burner and the ITB were run at their maximum exit temperatures, and for the partial throttle case the ITB is used to augment engine performance up to the maximum ITB exit temperature.

Figure 18 shows the results for the for the full throttle case for engine A and both engines exhibited similar performance. The ITB engines exhibit an increase in thrust over their conventional variant as Mach number increases. The ITB engines do have slightly higher fuel consumption due to the increased fuel flow to the ITB. Because TSFC does not increase for the ITB engines above $M = 1.1$ for engine A, and $M = 0.7$ for engine B, they have better performance at higher flight speeds. The change in slope for the thermal efficiency of the ITB engines is a product of limiting the main burner exit temperature.

21
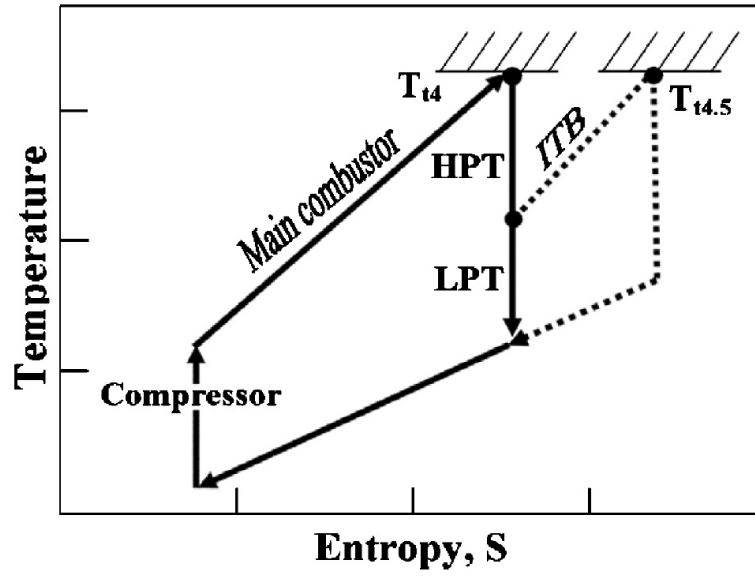
Figure 17: T-s Diagram of a Gas Turbine Engine with an ITB [15]

Figures 19 displays the results for the partial throttle study of engines A, and again the results for engine B were similar. As the throttle is decreased the ITB is turned off which presents as a discontinuity in the graphs. With the ITB off there is a sudden increase in TSFC and a decrease in thrust. For the partial study cases the ITB extends the engines operational range over that of the baseline engines. The data also shows that there may be cases in which it more fuel economical to operate the ITB at partial throttle settings thereby reducing the fuel burned while still achieving modeled thrust augmentation. The work conducted by Lieu et al. shows that an ITB engine operation at full throttle out performs a conventional engine and the ITB engine will achieve higher thrust at lower TSFC.

Zelina et al. [16] used the Anthenien UCC to experimentally explore its use in a reheat cycle aero engine. The experiment feed vitiated air to the UCC in an atmospheric test rig as shown in Figure 20, and is operated in much the same way as discussed in Section II.

(a)   (b)

(c)
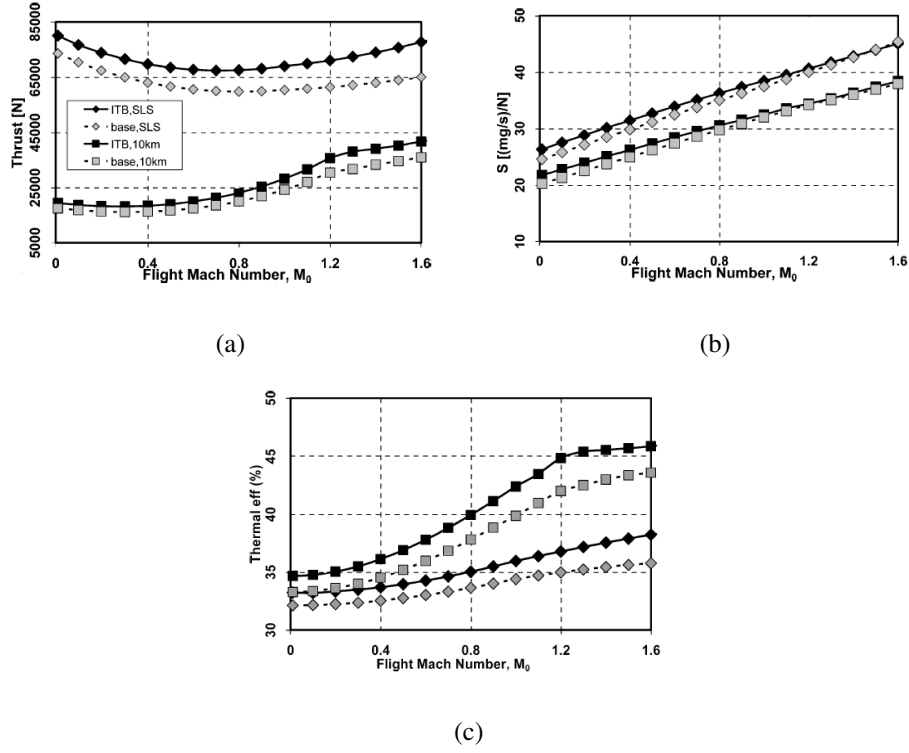
Figure 18: Full Throttle Comparison of Engine A [15]

(a)   (b)
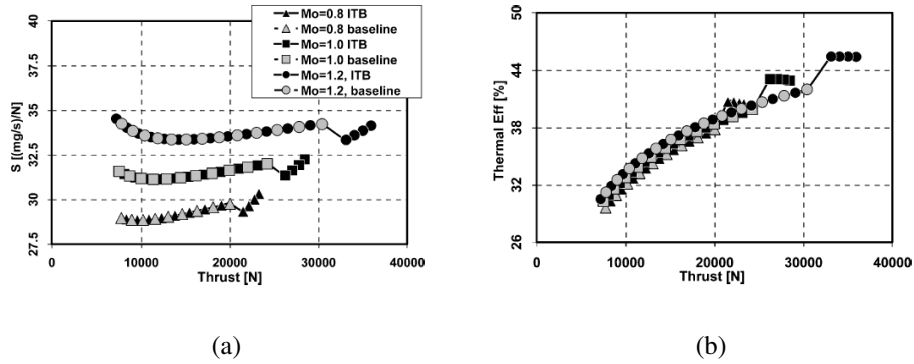
Figure 19: Partial Throttle Comparison of Engine A [15]

ITB pressure drops were varied between 2% and 3%, and the Overall Fuel/Air Ratio (OFAR) was varied between 0.0075 and 0.01 using JP-8 +100 as the fuel. Cavity airflow was kept constant at 20% of the total airflow. Cycle studies revealed an ITB will

23
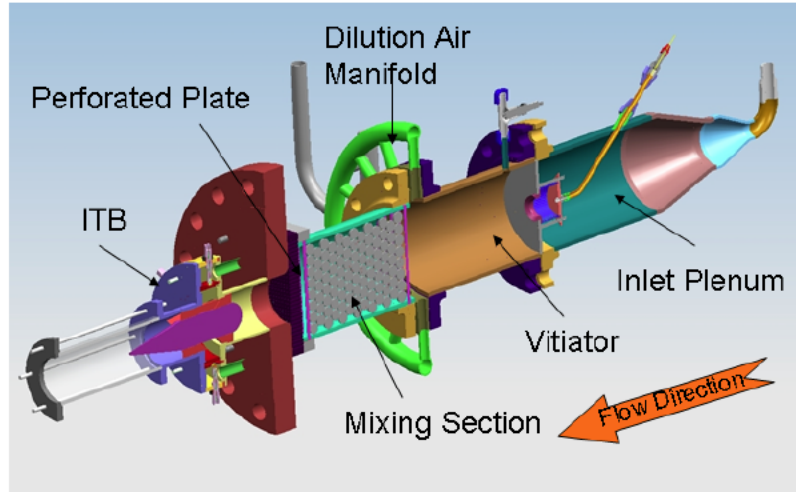
Figure 20: Experimental Test Rig with Vitiator and ITB Components Shown [16]

operate with a low temperature rise and therefore a low OFAR. The high-g combustion properties of the UCC can meet these unique ITB requirements. Combustion efficiency is plotted versus cavity ϕ at various levels of vitiated ϕ in Figure 21. At lean values of cavity ϕ, and low values of vitiated ϕ the combustion efficiency was between 85% and 95%. For all conditions the efficiency increased as cavity ϕ, and vitiated ϕ increased with value of 99% near a cavity ϕ of ~1.0. Data collected also indicated the combustion efficiency is a strong function of cavity g-loading, and g-loading can dominate the combustion efficiency even for low levels of cavity ϕ, as seen in Figure 22

Spytek [17] has demonstrated a working ITB engine utilizing a proprietary UCC design as an ITB. The ITB was fitted to an existing Spytek turbojet engine, and the 2nd turbine was connected to an axial booster fitted to the Spytek engine as shown in Figure 23. The diffuser design tested core mass flow splits from 0 to 50%, and determined an optimal flow split for this design to be 23%. This mass flow split stabilized ITB equivalence ratios between 0.6 and 0.7, while providing acceptable ignition characteristics. The ITB pressure drop was determined to be 4.4%, which is higher than the desired design point pressure drop of 3.75%. The increased pressure drop is attributed
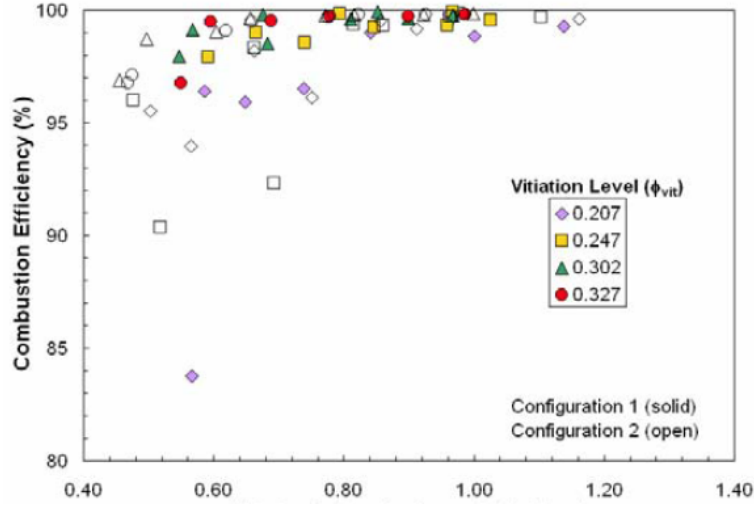
Figure 21: Combustion Efficiency as a Function of Cavity ϕ and Vitiation Level [16]
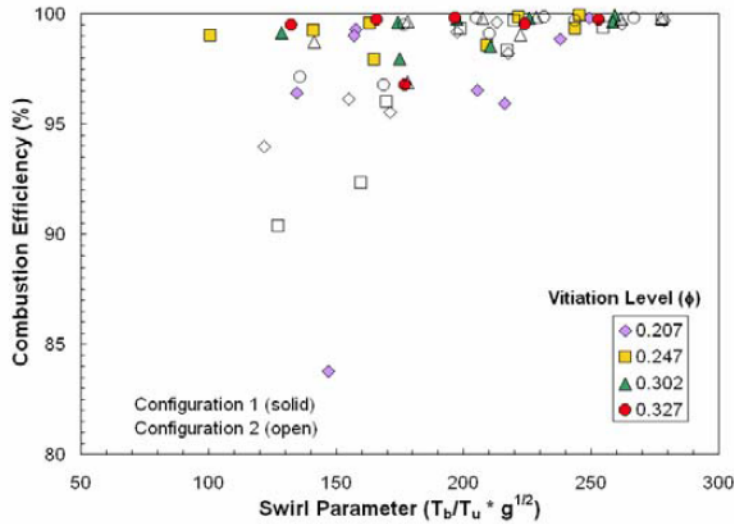
Figure 22: Combustion Efficiency as a Function of Swirl Parameter [16]

to the additional components present in the ITB design as compared to a conventional combustor. The system was able to achieve a 16% to 22% increases in power on demand from the engine with a moderate temperature increase across the ITB of 588 K. The second turbine used in this configuration was not cooled, and therefore possibly limited the power extraction that could be achieved from the ITB.

25
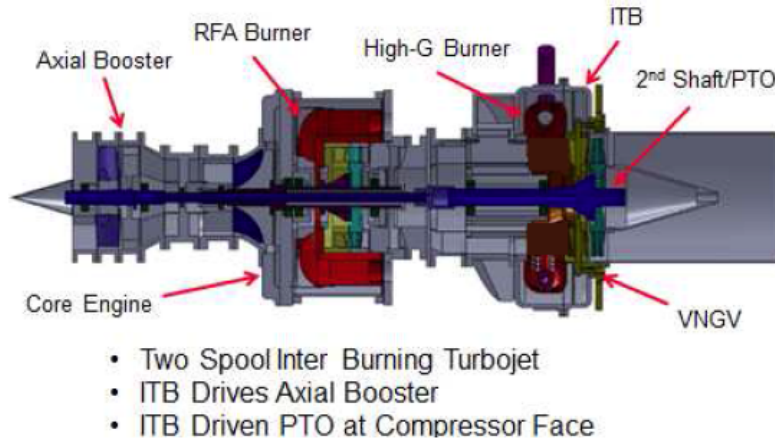
Figure 23: Spytek JI304-SA115B Gas Turbine with ITB [17]

Conrad et al. [18] has begun using the AFIT UCC as an ITB in an extension of the work done by Zelina et al. [16]. Conrad's work has been done in an effort to investigate and solve integration issues in using the UCC as an ITB. The first issue is to take a common vitiated flow source an split it between the core, and the cavity of the UCC. A diffuser has been designed to address this issue, and analysis has been conducted to determine the optimal flow split for this purpose. The second issue is designing the vane hardware to pull the hot combustion gasses out of the cavity, and back into the core flow. To achieve this a new UCC center body was designed. The flow path through the ITB is shown in Figure 24 which also shows the diffuser, and center body designs. Three diffusers mass flow splits were designed for the ITB. The core to cavity percentage mass flow splits chosen were 80/20, 70/30, and 60/40. The diffuser was designed to take in ~0.45 kg/s of vitiated air from the Small Turbine Engine (STE), and split the flow between the core and the cavity of the ITB. CHEMKIN was then used to determine which mass flow split may exhibit the best results. For the designed temperature gain in the ITB of 300K, and the three mass flow splits; the cavity equivalence ratios were determined to be 0.34, 0.45, and 0.67 respectfully. Additionally CHEMKIN was able to determine the 70/30 mass flow split would potentially yield the best emissions results.

26
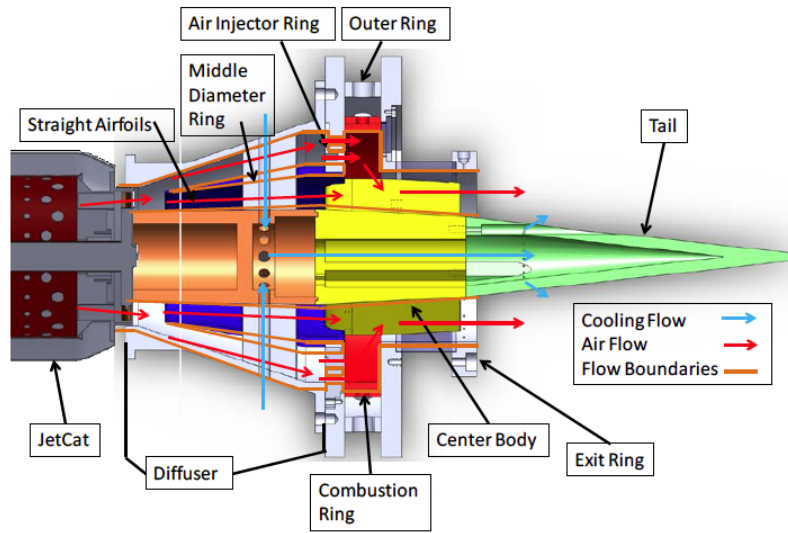
Figure 24: Flowpath Through the ITB Application [18]

Engine Modeling

The Numerical Propulsion System Simulation (NPSS) project was developed by National Air and Space Administration (NASA) in coordination with various other government agencies, academic institutions, and industry partners [19, 20]. NPSS is capable of performing complex aerothermomechanical computer simulations of gas turbine engines. The capability to realistically model complete gas turbine engine systems has the potential to accelerate the development of new engines and reduce the cost associated with full scale engine testing [19]. This technology can also be used in researching new, and potentially beneficial engine thermodynamic cycles, components, and control schemes. The NPSS code is currently used throughout industry to include companies such as General Electric (GE), and Pratt and Whitney (PW), and provides a common engine modeling code that can be used for collaborative efforts. Companies are currently using the NPSS system on engine programs such as the GP7200 (Airbus A380 joint GE, and PW), the F135 (Joint Strike Fighter (JSF) by PW), and the F136 (JSF joint GE and Rolls Royce) [21]. It has been estimated that NPSS can reduce design, and

development time by as much as 40%, and translates into a potential savings of $100 million in development time per year [20].

Until recently, modeling interactions between gas turbine engine components has been limited to two-dimensional analysis at best [20]. Most engine simulations are conducted at the zero, or one-dimensional level, and are not capable of capturing the multidimensional, and multidisciplinary flows that are found within a gas turbine engine. At its core, NPSS provides a zero-dimensional simulation environment with the added benefit of allowing the incorporation of higher fidelity component models by establishing data exchange standards between components. The NPSS environment allows for "zooming" between components of varying fidelity while operating at a zero-dimensional view of the engine [20].

NPSS is written in the computer language C++ which is an object-oriented programming language. Object-oriented languages aid in software development by allowing for maximum code reusability, clear data connectivity, and code modularity [20]. The modularity of the object-oriented structure of NPSS allows for nearly any conceivable engine architecture to be modeled [22]. NPSS is a very complex tool but its object-oriented nature allows for advantages in readable input, use-specified output, and modularity that allows for customization without having to modify the NPSS source code [22]. Like all object-oriented programming languages, NPSS is composed of basic building blocks, or classes. The five basic classes are elements, subelements, flow stations, ports, and tables. Examples of elements are compressors or turbines, and subelements would be a particular compressor map calculation within a compressor element. Flow stations carry out thermodynamic and continuity calculations. Ports are how elements are linked and consist of mechanical, fluid, fuel, data, and thermal ports. Tables access heat transfer equations and flow station properties [21].

Jones provides a comprehensive example of the use of the NPSS code for the zero-dimension analysis of a mixed flow turbofan capable of supersonic operation [22]. Figure 25 shows a block diagram of the Jones engine. In the case of a turbofan engine the four main design parameters that most effect the engine figures of merit, such as TSFC, ST, and thrust to weight ratio, are the Overall Pressure Ratio (OPR), combustor exit temperature, Fan Pressure Ratio (FPR), and BPR. The engine designer can vary one or more of these parameters and must be careful to note that varying any one parameter can have undesirable effects on the others. Aside from the four main design parameters, the other components parameters must be estimated for the engine model. These parameters include intel recoveries, component efficiencies, pressure drops, cooling bleed flows, power extractions, etc. For the on-design analysis of the engine conservation of mass, momentum, and energy must be met. NPSS can develop inconsistencies that must be resolved by the designer due to it's building block nature. In the case of mixer elements, it is assumed that the incoming streams must have equal static pressures in order to mix, and enthalpy, and force balances must be observed between the incoming and outgoing streams. Conservation of energy, or torque, across the component shafts must also be observed. The torque balance across the shaft can be accomplished by varying an independent parameter until dependent condition is met. The NPSS solver must solve a series of simultaneous equations in order to arrive at a valid solution. NPSS uses sets of independent and dependent variable pairs to construct the matrix of simultaneous equations that will be solved. Each independent is varied until the decided value of the dependent variable is met. There is no limit to the number of independent and dependent pair that can be specified. For the off-design analysis the sizing of the engine components accomplished during on-design analysis are now frozen. The engine is then run for conditions such as varied throttle setting, altitude, and flight speed to study the off-design performance of the engine.
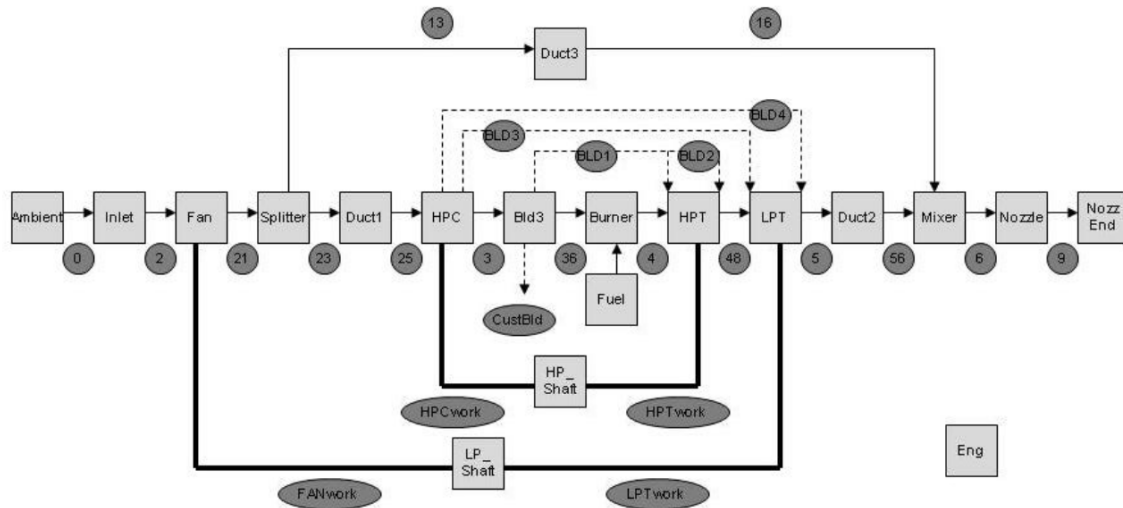
Figure 25: NPSS Mixed Flow Turbofan Model - Element and Link Names [22]

Although NPSS is a newer engine simulation code it has gained wide acceptance and has been used in numerous engine applications. Gomes et al. verified the performance of the NPSS code against two other engine simulations codes [19]. Dymola, MATLAB/Simulink, and NPSS were compared against one another, and to an older code, DIGTEM [23], which was written in Fortran circa 1983. The engine simulated was a two-spool, two-stream, low-bypass, augmented turbofan. All three simulations yielded almost identical results and compared well to the DIGTEM data. The engine simulations only significant difference was in computational time required, in which Dymola was the fastest, and NPSS was the slowest performer.

Corbett and Wolff used NPSS to model the transient effects on a dual bypass Variable Cycle Engine (VCE) [24]. Figure 26 showed a digram of the engine, including labeling of the variable components. Their research added time transient effect to the model originally developed by Simmons [25]. The transient effects modeled were inertial shaft dynamics, heat soak in the turbomachinery, and humidity within the turbomachinery.

NPSS allowed for the modeling and study of these transient effects on the dual bypass VCE, and was shown that the inclusion of time dependent analysis could be included without significant impact on other engine parameters.
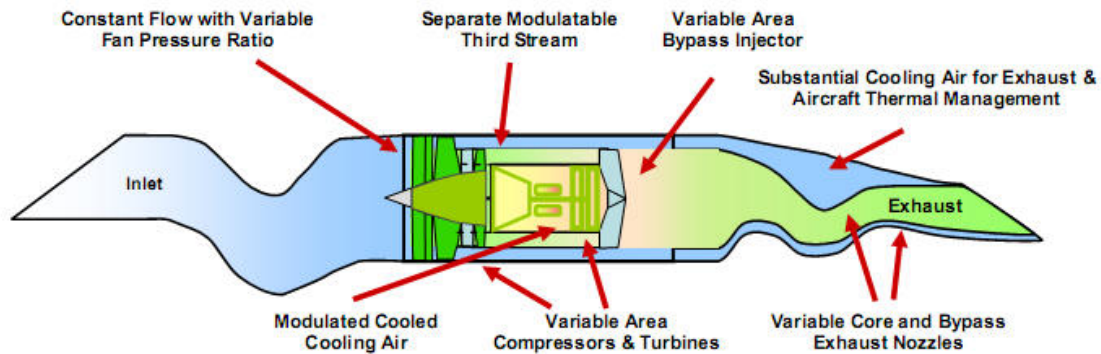
Figure 26: VCE with Variable Components Labeled [24]

Kestner et al. [26] used the NPSS code to develop a mission performance module that allows for collaborative analysis of engine and aircraft mission performance. They were able to take advantage of the object-oriented nature of NPSS, allowing them to expand the code beyond engine modeling and simulation. The newly developed model allows for the execution of an installed engine model analysis at any leg of a defined mission. This was accomplished though the creation of modular mission elements that allowed for the development of complete mission profiles. The modular nature of NPSS allows for engine, mission, or airframe analysis with minimal coding effort.

Huffman et al. [21] have also extended the use of NPSS beyond the scope of just the gas turbine engine. They have used NPSS to model an altitude test facility being built for the U.S. Army Research Laboratories Vehicle Technology Directorate. Figure 27 shows the block diagram of their NPSS model. Section 1 consists of the flow start elements and four compressors that provide mass flow to the facility and engine. Section 2 performed

temperature conditioning of the airflow using heat exchanges and associated components. Section 3 is used for ground testing and helps to further adjust the temperature of the airflow entering Section 4 from Section 2. Section 4 is ducting that is capable of switching between two different sources of airflow. Section 5 is the altitude test chamber, the engine from Section 7 is physically located in this section. Section 6 consist of the exhaust valves and ducting that will vent airflow back into the atmosphere. Section 7 can be any test article of interest. The model is capable of finding a converged solution for both the facility and the engine test article. The facility capabilities were demonstrated though parametric studies of the facility, and engine. During altitude test the engines power diminished by ~66% as the latitude increased from 1000 ft to 25,000 ft, as would be expected. The results of the simulation all be compared against the actual values of the built facility, and can also be used to test control methodologies for the facility.
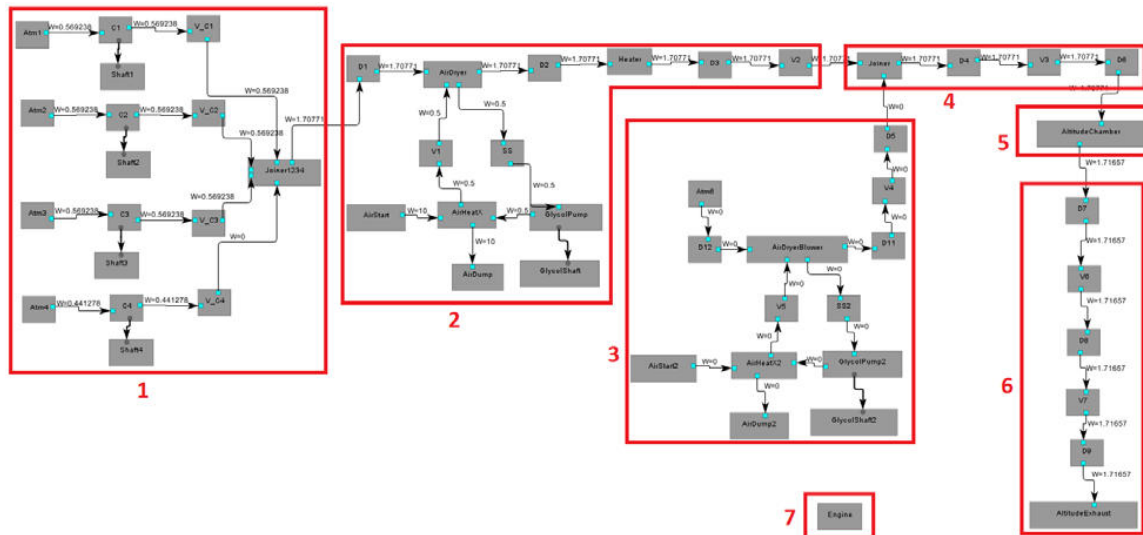
Figure 27: Altitude Test Facility [21]

III. Numerical Analysis

A numerical analysis was conducted using NPSS with the objective of determining potential applications for the proposed ITB engine cycle. This chapter discusses the development of the engine models used, and the results of the numerical investigation. The ITB engine model was compared against an engine model using a conventional afterburner for performance augmentation. The engines studied in this numerical analysis are comparable to an engine used for a large Unmanned Aircraft System (UAS). Engine model component parameters were kept identical to the maximum extent possible so useful comparisons could be made between existing afterburning engine technology and the potential ITB engine. The models used for this investigation were modified from an existing mixed stream turbofan model created by Simmons [25].

Engine Model Development

The modeled engines are high bypass turbofan engines modified to include an afterburner in one variant, and an ITB in another variant. Figures 28 and 29 show the block diagrams for the afterburing and ITB engines respectively. Common components were used between the two models to the maximum extent possible, e.g., pressure ratios, efficiencies, and pressure drops. The baseline engines are mixed stream turbofans with an air mass flow of 136 kg/s at sea level. The compression section consisted of one fan and one High Pressure Compressor (HPC) that together produce an OPR of 23 with a BPR of 4.4 for the afterburning model, and 3.4 for the ITB model, and an FPR of 1.84 at the design point. The model has two turbine sections with the HPT driving the HPC and the LPT driving the fan. Cooling is provided to both the HPT and the LPT by bleed air taken form the HPC. Power is extracted from the LPT shaft, and the baseline engine has a

33

constant 49.96 kW load applied. The maximum cycle temperature for the models is ~1600 K.

Engine Model Specifications.

The baseline engines were designed to produce approximately 44.5 kN of thrust (dry) at sea level, and operate at an altitude of 10.7 km, and at a Mach number of 0.6 at 100% fan speed. As with any mixed steam turbofan, a mixer is used to balance the pressures, and recombine the core and bypass flows. A requirement placed on the mixer is the total pressure in the bypass stream must remain higher than the total pressure in the core stream, and the static pressures in both streams must also match. This is accomplished by calculating an R_{mix} value from Equation 4. Slight differences exist between the ITB engine and the afterburning engine models. The most notable differences are the locations and specifications of the additional burners, and the difference in bleed cooling from the HPC used to cool the LPT. The engine component specifications are listed in Table 1.

$$R_{mix} = \frac{P_{t_{bypass}}}{P_{t_{core}}} \tag{4}$$
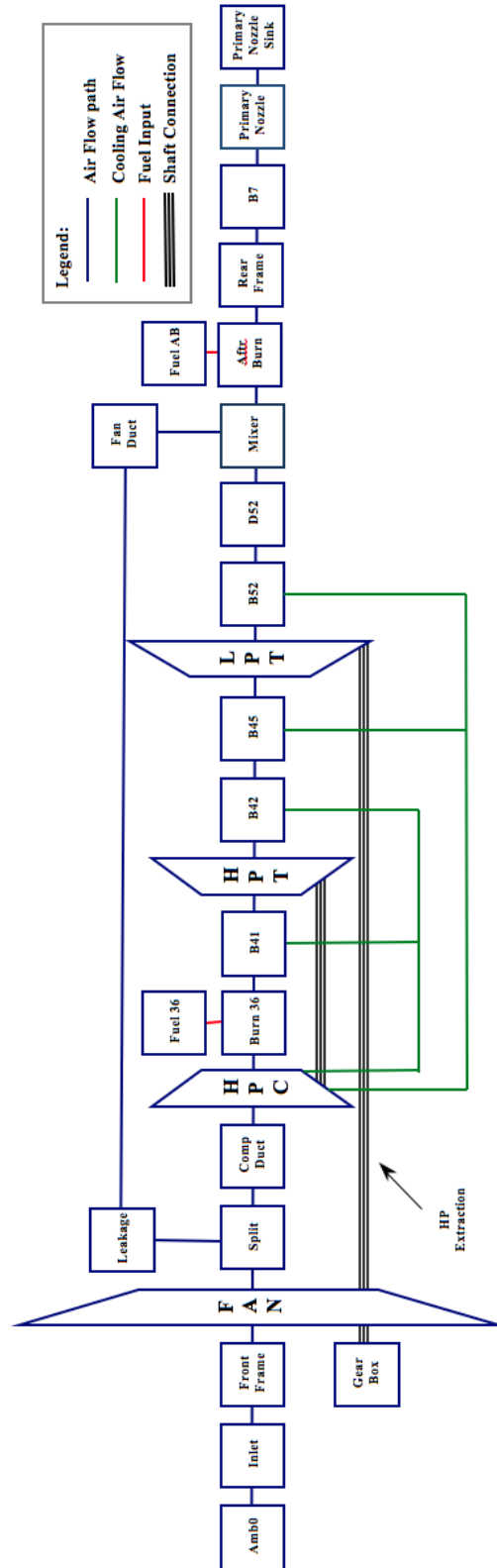
Figure 28: Block Diagram of Baseline Engine with AB

Figure 29: Block Diagram of Baseline Engine with ITB

Table 1: Engine Model Component Specifications

Parameter	Afterburner (AB) Engine	ITB Engine
Inlet ram pressure recovery	0.99	0.99
Front frame dP/qP	0.1	0.1
FPR	1.8	1.8
Split BPR	**4.42**	**3.41**
Leakage	0	0
Fan duct M	0.3	0.3
Fan duct dP/qP	0.032	0.032
Compressor duct M	0.5	0.5
Compressor duct dP/qP	0.01	0.01
HPC Pressure Ratio (PR)	13.53	13.52
Burner (Burn36) M	0.2	0.2
Burner (Burn36) dP/qP	0.04	0.04
Burner (Burn36) Efficency	0.9995	0.9995
Bleed (B41) non-chargeable	0.1	0.1
HPT PR	4.667	4.667
Bleed (B42) chargeable	0.05	0.05
ITB dP/qP	N/A	**0.04**
ITB efficency	N/A	**0.99**
Bleed (B45) non-chargeable	**0.05**	**0.1**
LPT PR	2.029	2.029
Bleed (B52) chargeable	**0.02**	**0.05**
Duct (D52) M	0.2	0.2
Duct (D52) dP/qP	0.02	0.02
Mixer M	0.4	0.4
Mixer R_{mix}	1.05	1.05
AB dP/qP	**0.02**	N/A
AB efficency	**0.97**	N/A
Rear frame duct M	0.4	0.4
Rear frame duct dP/qP	0.03	0.03
Bleed (B7)	0	0
Nozzle C_{fg}	0.95	0.95
High Pressure (HP) spool PX (kW)	0	0
Low Pressure (LP) spool PX (kW)	49.96	49.96

First is an on-design case where the thrust required at sea level, the OPR, and the maximum turbine inlet temperature are specified. At the design point, the models are allowed to vary BPR as a dependent variable to allow the model to converge on a solution. The models are then run off-design at the same design point as the on-design case. This

matching case is used to verify that the off-design case matches the on-design case for the same conditions. Subsequent models are adjusted to 0.2 Mach at sea level and then run at an altitude 1.5 km. At an altitude of 1.5 km, the model's Mach number is increased to $M = 0.4$, and then run at the final altitude of 10.7 km. Once at the desired altitude, the model is run to 0.6 Mach to reach the Point of Interest (POI) for this investigation. The baseline engine performance specifications are tabulated in Table 2 with the performance values at the baseline conditions for the parametric studies. The minor differences in performances are a result of the greater pressure drop and LPT cooling bleeds required of the ITB model. The ITB engine is sized with a greater pressure drop and cooling bleed; and therefore, represents a model of a slightly larger engine.

Table 2: Engine Performance Specifications (Dry)

	AB SLS	ITB SLS	AB POI	ITB POI
Thrust max (N) [Dry]	44482	44460	7740	7870
Tt4 (K)	1601	1600	1343	1337
OPR	23	23	23.5	23.4
BPR	4.42	3.41	4.35	3.36
TSFC (kg/N*hr)	0.0459	0.0513	0.0703	0.0772
Weight Flow (kg/s)	136	136	136	136

Afterburning Model.

As shown in Figure 28, the afterburing model has the additional burner located after the mixer, and uses a non-variable mixer design. An R_{mix} value of 1.05 was chosen at the design point to size the mixer. The pressure drop across the additional burner is 2% with an isentropic efficiency of 97% [27]. Cooling of the LPT consists of 7% of the core flow, which is approximately half that used to cool the HPT.

ITB Model.

In the ITB, shown in Figure 29, the additional burner is located between the HPT and the LPT just after the chargeable HPT cooling bleed, B42, and just before the non-chargeable LPT cooling bleed, B45. In order to meet the desired R_{mix} value, the ITB model required the use of a Variable Area Bypass Injector (VABI) mixer because energy is added to the cycle prior to the mixer during augmentation. The variable area mixer varies the bypass flow area while keeping the total mixer inlet area constant. This allows for a favorable pressure gradient to be achieved between the core and bypass flows. The pressure drop across the additional burner is 4% with an isentropic efficiency of 99%. Cooling the second turbine cannot be neglected with the use of an ITB. The ITB can potentially raise the temperature into the LPT to the same temperature as the HPT. To meet this objective additional cooling is supplied to the ITB shown in Table 1.

Parametric Studies.

Three parametric studies were conducted to investigate potential applications for the ITB engine cycle. The ITB cycle is compared against an afterburning cycle for use in augmenting thrust and power extraction. The ITB pressure drop was investigated to determine the range of pressure drop the ITB should achieve to outperform the afterburning cycle in fuel efficiency.

The thrust and Power Extraction (PX) augmentation studies begin with the models in a non-augmented condition, with the afterburning and ITB engine models capable of producing 7740 N and 7870 N of thrust at military power, respectively. Fuel flow to the additional burner is varied to increase thrust in increments of 44.5 N. The case of augmented power extraction is conducted similarly as the case of thrust augmentation. The model is run at the same starting condition as the increased thrust case and fuel is allowed to flow into the additional burners to meet the increased shaft power demand. The models are designed so additional shaft power can only be extracted from the low pressure spool.

ITBs are expected to have larger pressure drops when compared to the pressure drop across an afterburner. To study the affect this may have on performance the pressure drop is varied at the same initial conditions as before. The engine is not resized at the design point for each change in pressure drop across the ITB. The baseline ITB engine is run at the desired initial conditions, and then the pressure drop is varied on the original size baseline engine.

Numerical Results

The objective of this numerical analysis is to determine the best application for the ITB engine cycle, in terms of fuel efficiency, when compared to a conventional afterburning engine cycle. The results of the numerical analysis consist of a thrust augmentation, and a PX augmentation study of an ITB engine versus an afterburning engine. These studies seek to determine the best application of the ITB when used for engine performance augmentation. The numerical results of the effects of ITB pressure drop are also presented in this section. The pressure drop study seeks to explore the range of pressure drops an ITB can possess and still provide acceptable performance augmentation.

Numerical Thrust Augmentation Investigation.

The thrust augmentation study begins at the POIs from Table 2. To increase thrust in increments of 44.5 N, the models, shown in Figures 28 and 29, are allowed to vary fuel flow into the additional burner. Figure 30(a) shows the relationship between a increased thrust relating to an increase in TSFC for both the afterburning and ITB models. As a basis of comparison the ITB temperature rise of 588K experienced by Spytek [17] was used to determine if the results achieved by the ITB model are reasonable.

As expected, both engines suffer from an increase in TSFC as fuel is used in the additional burner to achieve the desired increase in thrust. However, the ITB did yield significantly better results with a much lower rate of TSFC increase when compared to the

40

afterburning model. The ITB model is slightly less fuel effect than the afterburning model prior to thrust augmentation, but after ~700 N of additional thrust the ITB becomes more fuel efficient than the afterburner. The results for the ITB model were accomplished with a modest total temperature increase between the HPT and the LPT shown in Figure 30(b). The ITB model provides a ~4500 N increase in thrust with an ITB ΔT_t of 565K. This temperature rise is consistent with the experimentally determined temperature rise recorded by Spytek.

(a) TSFC vs. Thrust   (b) ITB ΔT_t vs Thrust
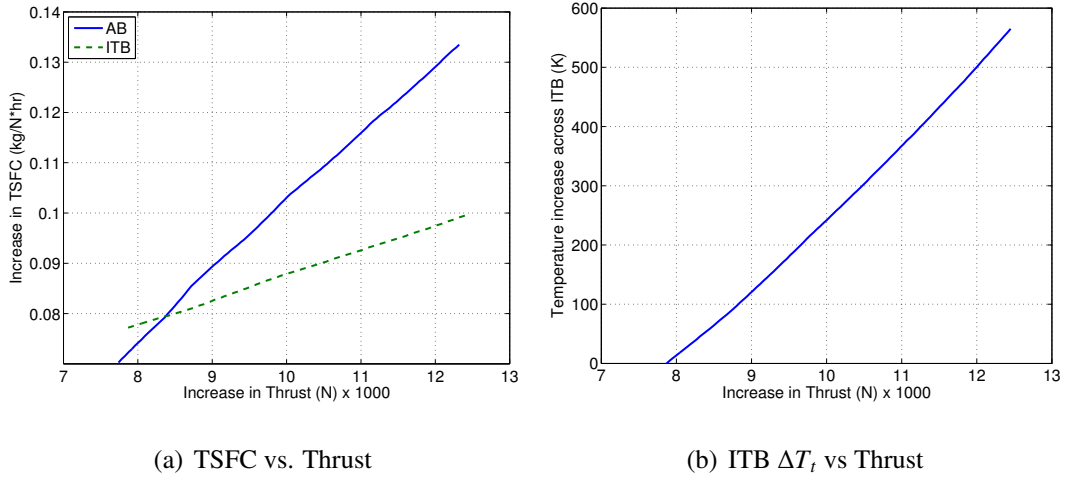
Figure 30: Thrust Augmentation Performance Benefits

Despite the desired result of improved TSFC of the ITB model versus the afterburning model there are some concerning results to be mentioned. While the ITB engine did have better TSFC results it came at the cost of fan efficiency and HPC stall margin encroachment. The model is forced to reduce the fan efficiency to compensate for the fan overspeed caused by the increased LP shaft speed which is a result of the ITB temperature increase. The efficiency reduction is a way of trying to control the pressure rise in the core flow in order to achieve the requirements placed on the mixer. In order to achieve a R_{mix} value of 1.05 the engine model increases the bypass ratio and lowers the fan

efficiency to decrease the OPR in the core flow. The requirement of having an R_{mix} value greater than one prevents flow reversal in the bypass stream that can lead to stalling the fan. While the ITB model will continue to converge on a solution for negative values of stall margin this study is terminated at the point where the HPC has reached a stall margin of zero. Due to the mixing requirement the ITB model is not capable of reaching increases in thrust much greater than 55% while the afterburning model would continue to provide performance well beyond that of the ITB model. The negative effect on fan efficiency and stall margin for the ITB model can be seen in Figures 31(a) and 31(b) respectively.

(a) Component Efficiency vs. Thrust

(b) HPC Stall Margin vs. Thrust
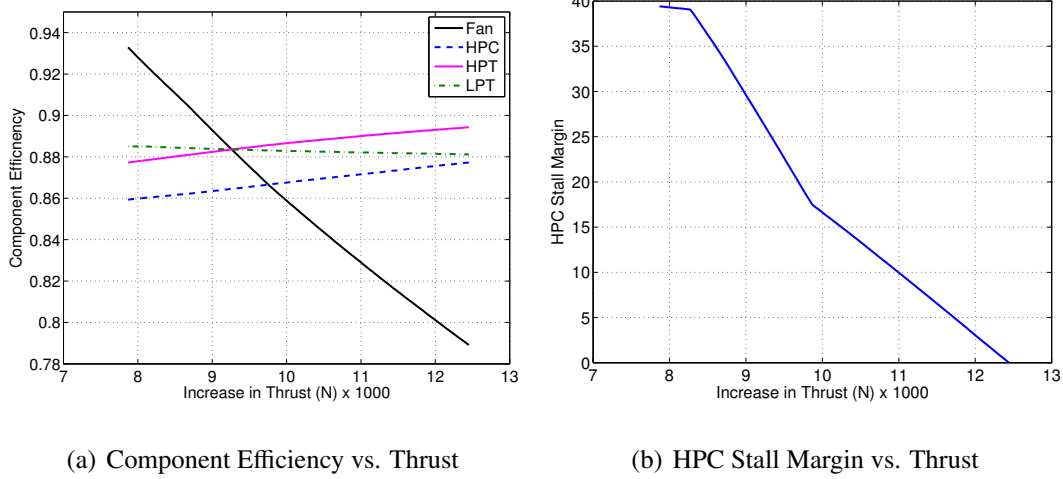
Figure 31: Thrust Augmentation Performance Consequences

The undesirable trend in the ITB model performance can be attributed to the mixer. The afterburner model has the additional burner located down stream of the mixer; therefore, adding energy to the system does not change the engine characteristics prior to the mixer. The ITB model does not share this same benefit, and even with a VABI mixer performance is still limited. The negative effects experienced by the ITB could be avoided if the fan overspeed condition is controlled, and the mixing requirement is removed. The

ITB concept may provide better thrust augmentation results when used with a separate stream turbofan engine equipped with a geared fan.

Figure 32 shows the T-s diagram for the ITB engine cycle core stream at various levels of thrust augmentation. The work of the cycle is the area under the curve of the T-s diagram. As expected the work performed by the cycle increases as thrust augmentation increases. For the case of maximum thrust augmentation of 12450 N, the ITB reaches the maximum cycle temperature of 1600 K. The point at which the ITB cycle becomes more fuel efficient than the afterburning cycle, as shown in Figure 30(a), occurs at a thrust value of ~8400 N. Figure 32 shows that only a small increase in temperature across the ITB is necessary for the ITB cycle to begin to outperform the afterburning cycle. The increases in the main burner temperature with increased thrust augmentation is attributed to the loss of LPT efficiency experienced by the engine model, as shown in Figure 31(a). The loss in LPT efficiency could potentially be avoided if the engine was designed to handle the added energy supplied the ITB.
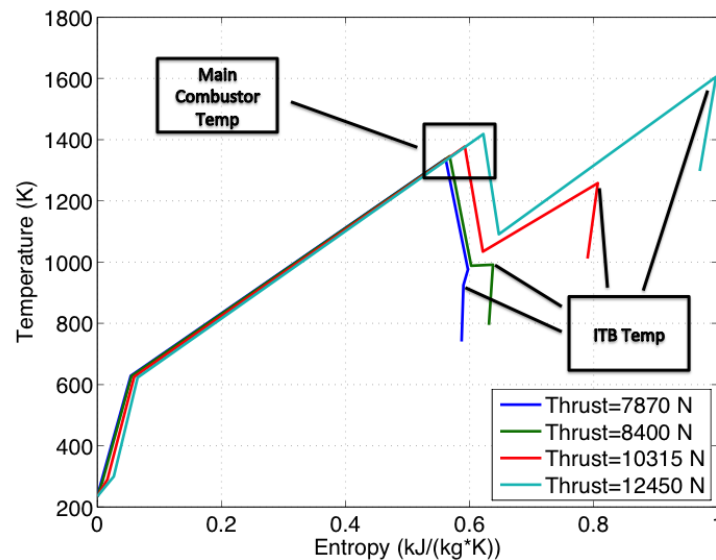
Figure 32: T-s Diagram for ITB Thrust Augmentation

Numerical PX Augmentation Analysis.

For the PX augmentation study the engines are undergoing a constant power demand from the aircraft. The aircraft demands more power from the engine to accommodate additional electrical loads such as operating sensors or weapons. The PX augmentation study begins with both engines at the same POI condition as the thrust augmentation study. The engines are consuming ~50 kW of power at this condition, and additional shaft power is demanded from the LP spool of the engine models. The models are required to maintain thrust by increasing the fuel flow to the additional burners to accommodate incremental increases in PX of ~7.5 kW. Small increases in power extraction were used to minimize model convergence issues.

Figure 33(a) shows the ITB maintains it advantage in TSFC over the afterburning engine. For an PX increase of 500 kW, the ITB engine has a 30% less increase in TSFC than the afterburning engine. This margin continues to widen as more PX is demanded of the engine models. The ITB engine model was able to achieve these results with a modest ~174 K temperature increase across the additional burner, shown in Figure 33(b).

(a) TSFC vs. PX   (b) ITB ΔT_t vs PX
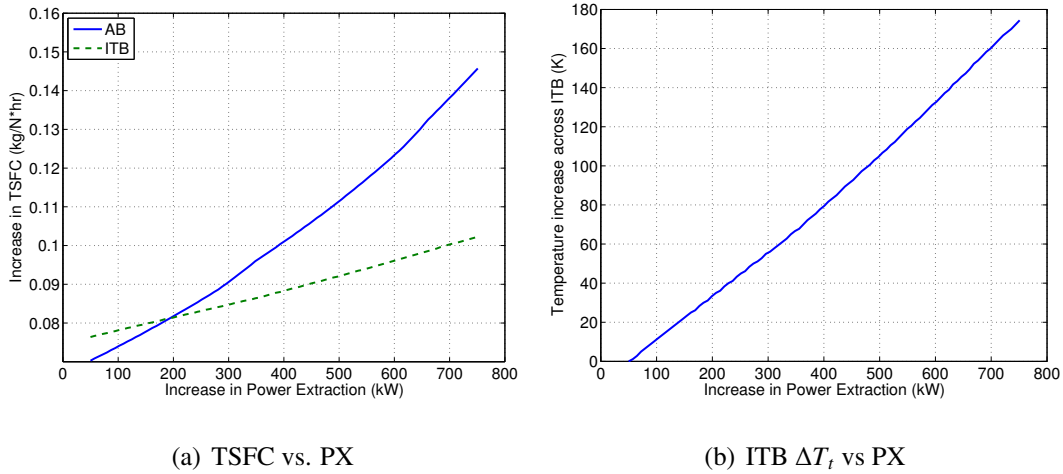
Figure 33: PX Augmentation Performance Benefits

In addition to the benefit in TSFC achieved by the ITB engine model PX augmentation does not suffer from the same consequences that effected the thrust augmentation case. Figure 34 shows no significant decreases in turbo machinery component efficiencies with only a very slight change in HPC stall margin. These results can be attributed to the enthalpy increase, caused by the ITB being primarily used by the LPT to meet the increased PX demanded of the LP spool. With most of the additional energy being used as shaft power the fan does not experience the overspeed condition of the thrust augmentation case.
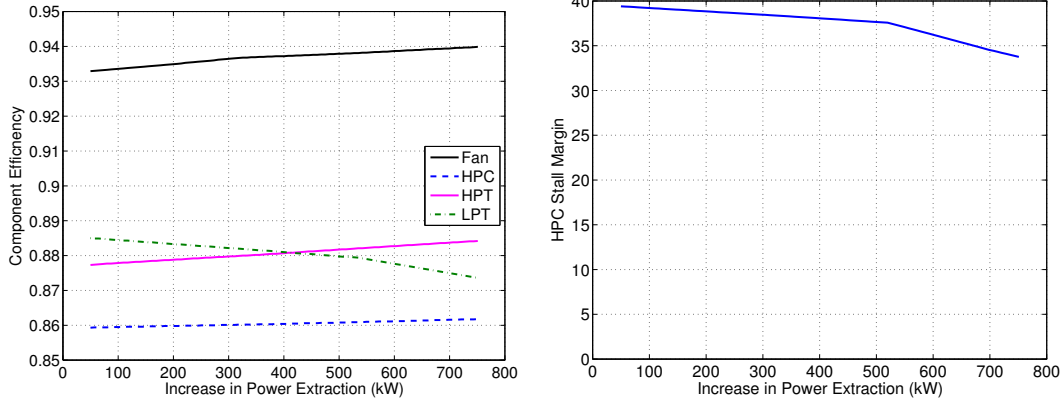
(a) Component Efficiency vs. PX   (b) HPC Stall Margin vs. PX

Figure 34: PX Augmentation Added Benefits

The temperature in the ITB is a concern, it should not increase the maximum temperature of the engine cycle greater than the limit placed on the engine's main burner. The burners are limited by the inlet temperatures into the HPT and the LPT with a maximum Turbine Inlet Temperature (TIT) of 1600 K. Figure 35 shows the ITB never approached this temperature restriction, and the LPT required less bleed cooling than the HPT.
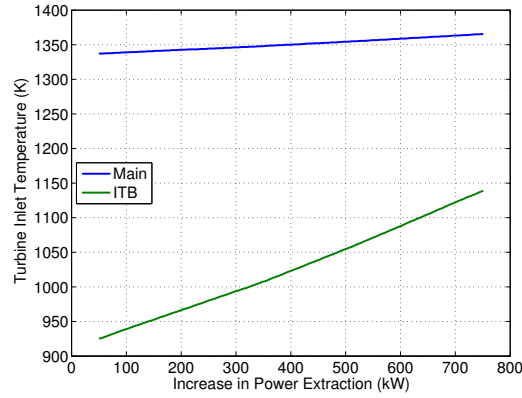
Figure 35: HPT TIT and LPT TIT During PX Augmentation

Figure 36 shows the T-s diagram for the ITB engine model core stream at various levels of power extraction augmentation. In the case of PX augmentation, the temperature rise in the ITB never exceeds the temperature in the main burner, and the cycle temperature remains below the maximum cycle temperature of 1600 K for all cases. At a PX augmentation of 155 kW the ITB engine is equal to the afterburning cycle in terms of fuel efficiency, and required a very small temperature increase across the ITB to achieve this result. As in the case of thrust augmentation, the increase in main burner temperature with increased performance augmentation is attributed to the loss of LPT efficiency seen in Figure 34(a).

ITB Pressure Drop Analysis.

To study the effect that the pressure drop across the ITB can be expected to have on engine performance, the PX study was accomplished with various ITB pressure drops. The baseline ITB engine model has a pressure drop of 0.04, and in addition to the baseline engine pressure drop, pressure drops of 0.08, 0.12, and 0.20 were also tested. ITB pressures drops are expected to be between 0.03 and 0.05, but significantly larger pressure drops were included to study the worst case pressure drop. Figure 37 shows the results of the effect of pressure drop on the TSFC vs PX performance of the ITB engine model. The
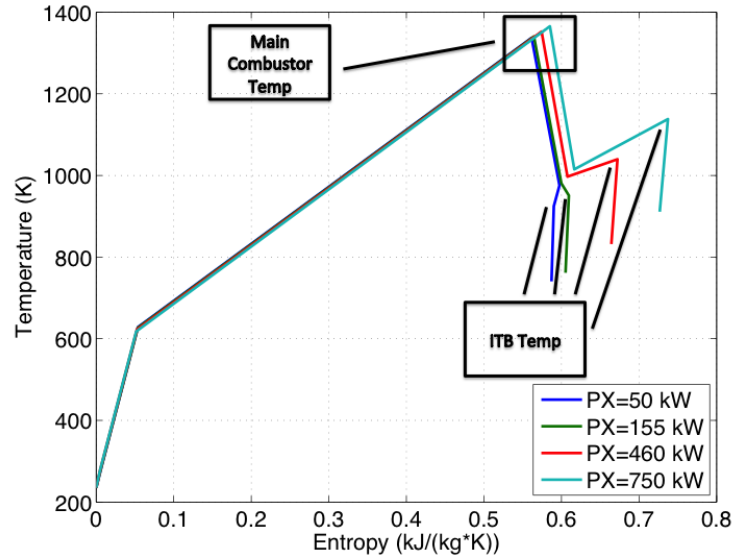
Figure 36: T-s Diagram for ITB PX Augmentation

data shows as the pressure drop increases, the ITB engine becomes less fuel efficient, and the point where the ITB becomes more fuel efficient than the afterburner requires a higher power extraction. Figure 37 shows the trend as TSFC relates to an increase in PX, and displays that the rate of TSFC increase is less than the afterburning case for all pressure drops examined. The lowest pressure drop of 0.04 was found to have the best performance results. Each pressure drop also exhibited the same modest temperature increase across the ITB, demonstrated previously in Figure 33(b).

Minor negative effects of increased pressure drop across the ITB become evident as the pressure drop effects on component efficiencies is studied. Figure 38 captures the effect of pressure drop on each of the turbo machinery components. A slight decrease in LPT efficiency is seen for each increase in pressure drop. This effect is most likely caused by the increased pressure drop in the ITB, reducing the amount of pressure available at the LPT for power extraction.

Figure 39 show the T-s diagram for the ITB, with pressure drops of 0.04, 0.08, and 0.20, at the maximum PX augmentation value of 750 kW. For all cases the ITB model is

47
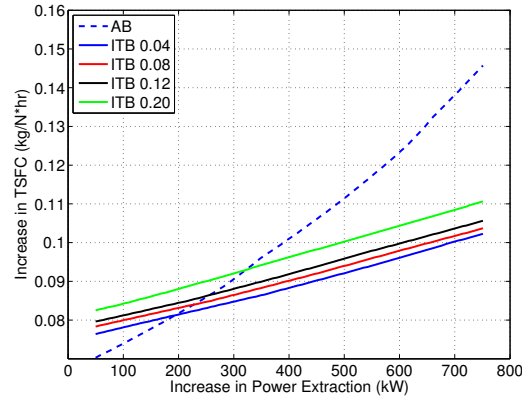
Figure 37: TSFC vs PX for Various ITB Pressure Drops

providing the same level of PX augmentation, but the ITBs with a pressure drops of 0.08 and 0.20 performed more work to achieve the same result. This demonstrates the work required to achieve an increase in power extraction increases with ITB pressure drop.

The most notable problem with increased ITB pressure drop is the significant increase in HPC stall margin encroachment for each increase in pressure drop. These results are shown in Figure 40, which shows the pressure drop increases the stall margin is significantly reduced. The promising result from this study is for the range of pressure drops expected of an ITB, from 0.03 to 0.05, the ITB engine performance is acceptable and is superior to the afterburning model.

(a) Fan

(b) HPC

(c) HPT

(d) LPT
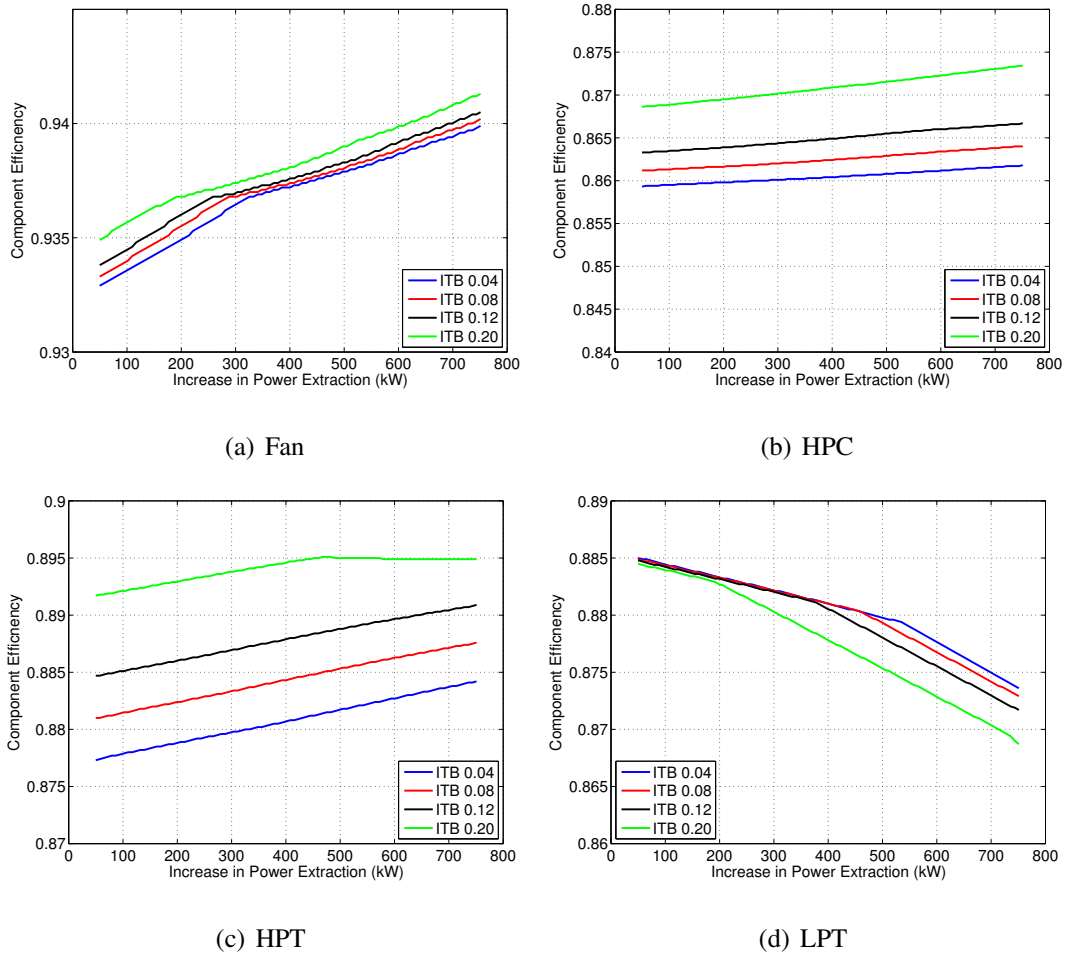
Figure 38: Component Efficiencies for Various ITB Pressre Drops
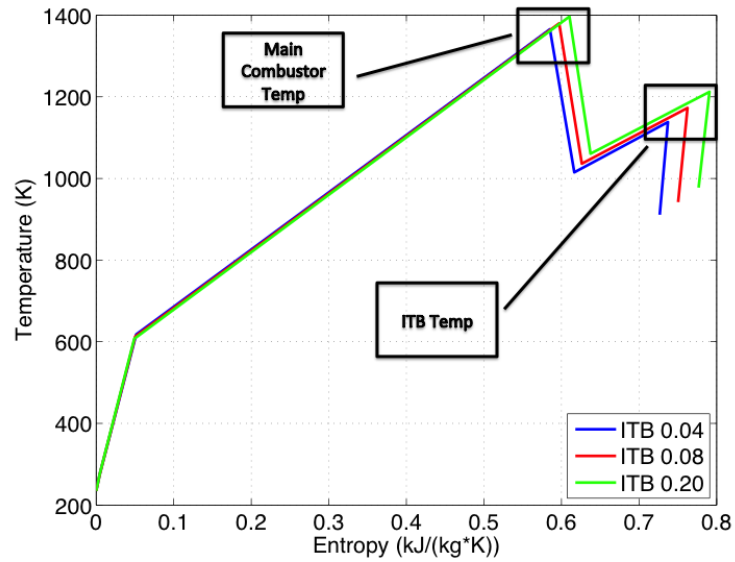
Figure 39: T-s Diagram at Various ITB Pressure Drops (PX=750 kW)
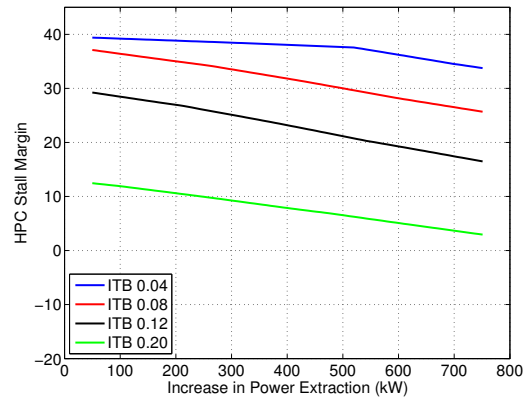
Figure 40: HPC Stall Margin by for Various ITB Pressure Drops

IV.   AFIT ITB Integration

In an effort to capitalize on the theoretical benefits associated with the ITB cycle, steps have been taken to integrate the AFIT UCC to accept a common flow source. The common flow source is necessary to expand the UCC concept to perform as an ITB. This work focuses on a continuing effort to investigate the use of the AFIT UCC for the purposes of exploring the ITB engine cycle. This work builds on the study done by Conrad [28] to characterize an ITB. First, the source of vitiated air to be used in the AFIT ITB configuration was tested to determine the baseline thrust performance. The baseline thrust of the JetCat P200 will be used for comparison to future AFIT ITB designs. Secondly, the common flow source diffusers designed by Conrad were tested to determine the actual performance. For the ITB concept to move forward the ability to utilize a common flow source for the core and cavity flows is necessary. The AFIT UCC currently utilizes separate flow sources for the combustor core and cavity flows. In an actual gas tubing engine application, the core and cavity flows will have to be taken from a single combustor inlet core flow.

ITB Configuration

The primary experimental component of this work incorporates a diffuser that takes a common source mass flow and divides the flow between the ITB combustion cavity and core flow paths. The ITB configuration used in this experiment, with component identification, can be seen in Figure 41. The components unique to the ITB configuration consist of a diffuser, air injection plates, center body, and combustion ring. The components of the ITB configuration will be discussed fully in the sections that follow.
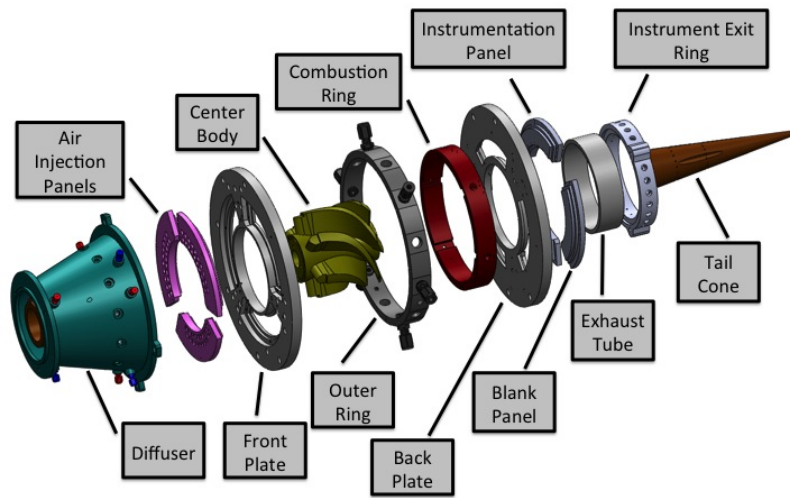
Figure 41: ITB Configuration with Component Identification

Inlet Air Flow.

The ITB is capable of using either facility supplied compressed air or a vitiated air source provided by the STE. The facility compressed air source is primarily used to supply the air mass flow to the ITB for experimental determination of the diffuser mass flow splits and core/cavity pressure drops. The vitiated air source is used for testing of the AFIT UCC operating as an ITB. Additional fuel can be added to the vitiated air in the circumferential cavity to simulate a second burner. Figure 42 show the air flow path through the ITB configuration.

Compressed Air.

Compressed air is provided to the ITB by a dedicated 50 hp Ingersoll Rand H50A-SD compressor capable of providing 1 kg/s of air at atmospheric pressure [29]. A layout of the compressed air supply configuration can be seen in Figure 43. Air from the compressor tank is provided through a 7.62 cm line and is controlled by a Flowserve MaxFlo 3 valve that limits the maximum mass flow rate to 0.6 kg/s. A Fisher 99 pressure
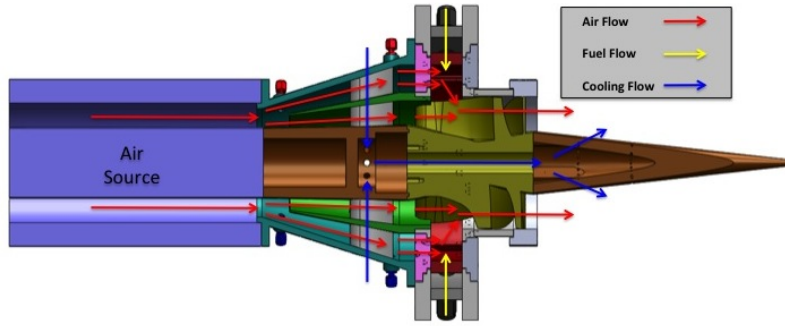
Figure 42: ITB Configuration Fluid Flow Diagram

reducing valve is used to reduce the compressor line pressure so the desired mass flow could be achieved. An FT2 Fox Thermal Instruments mass flow meter is used to measure the in-line mass flow and provide the information to the ITB control station. Control of the mass flow rate in the air line was achieved through the use of a Eurotherm 2404 PID controller, which can be manipulated from the control station through LabVIEW. The inlet air supply is instrumented with total and static pressure probes and a thermocouple probe to measure temperature, which is used to calculate the inlet air mass flow to the ITB. The facility is also supplied with 3.81 cm and 1.91 cm compressed air lines provided by the AFIT facility compressors. These line are capable of providing mass flows of 0.3 kg/s and 0.03 kg/s respectively. The smaller lines are primarily used in UCC testing that does not require a single mass flow source, and are therefore not used in this experiment.

Small Turbine Engine.

The vitiated air source selected for this experiment was the JetCat P200 STE, shown in Figure 44. The JetCat P200 is primarily used in the model aircraft community to power scaled jet aircraft. The AFIT UCC was originally designed to support an air mass flow of 0.45 kg/s [29] therefore, the STE was selected for its ability to provide ~ 0.45 kg/s of vitiated mass flow at full power. The full manufacturer specification for the JetCat P200 are shown in Table 3.
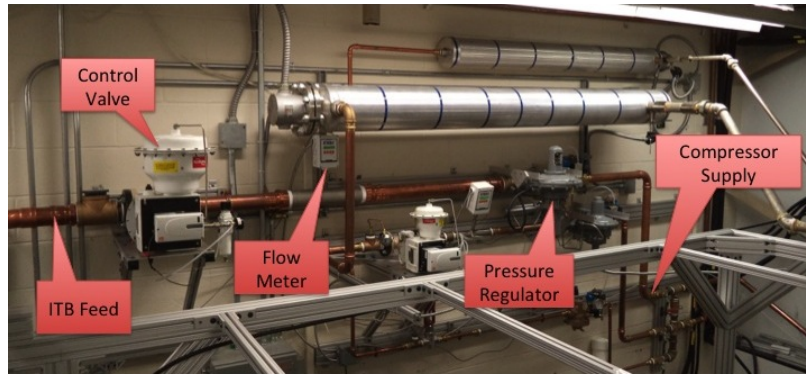
Figure 43: Compressed Air Configuration on North Wall of COAL Lab
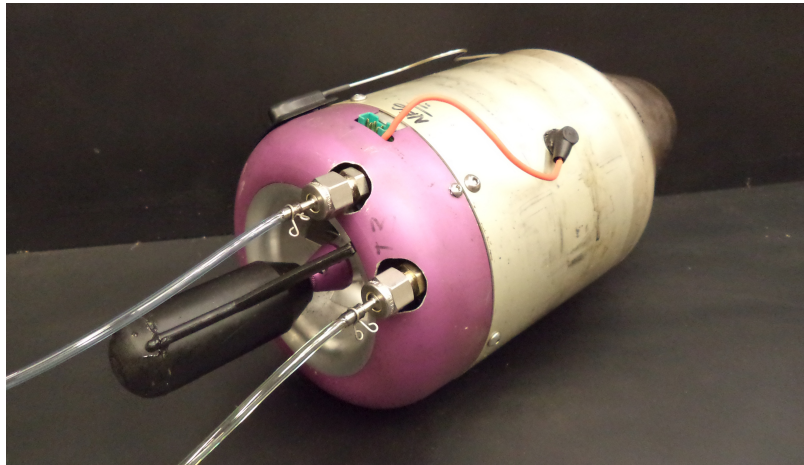
Figure 44: JetCat P200 STE

Fuel and electrical connections were made in accordance with manufacturer instructions provided in the JetCat Instruction Manual [31]. During operation, the JetCat P200 uses MSR IsoPro as a starting fuel, which is an 80% to 20% mixture of isobutane and propane. Once started, the STE operates on a 4 to 1 mixture of JP-8 and Aeroshell 500 turbine oil. The JP-8 fuel and oil mixture is contained in a 19 liter stainless steel Alloy Products Corporation general purpose vessel tank, and is pressurized with nitrogen to ~ 41.4 kPa to supply fuel to the JetCat fuel pump. Electrical power was provided through the use of a TENMA 72-7700 power supply capable of providing the high starting

Table 3: Manufacturer Rated Performance Specifications of the JetCat P200 [30]

Engine Performance Parameter	Manufacturer Rating
Speed Idle (rpm)	33000
Speed maximum (rpm)	112000
Thrust Idel (lbf)	2.0
Thrust maximum (lbf)	50.0
EGT minimum	480
EGT maximum	750
Pressure ratio	4.0
Total mass flow (lb/s)	1.0
Exhaust gas velocity (m/s)	490
Power output (hp)	72.1
Fuel consumption at idle speed (lb/hr)	13.46
Fuel consumption at maximum speed (lb/hr)	76.16
TSFC at idle (lb/hr*lbf)	6.66
TSFC at maximum (lb/hr*lbf)	1.54
Engine weight (lb)	5.22
Engine outer diameter (in)	5.20
Engine overall length including starter (in)	13.98

current demanded from the electric starting motor. The STE can be controlled using either the JetCat Ground Support Unit (GSU), or the AFRL supplied LabVIEW Virtual Instrument (VI). Instructions for operating the JetCat P200 with the GSU can be found in the JetCat Instruction Manual [31], and interactions how to use the LabView VI control interface is listed in Appendix A.

The JetCat P200 is sensitive to several variables affecting its ability to start. The glow plugs used with the STE should be a non-idle bar Rossi RT8 Extra Cold glow plug with

one coil exposed from the glow plug chassis. Even with the correct glow plug installed and configured, if start-up fails, the glow plug should be tested in accordance with manufacturer instructions. Colder ambient temperatures have a negative effect on start-up by reducing the starting gas pressure and causing compressor and turbine interference issues. Keeping the STE and starting gas at room temperature reduce these potential startup problems. It should be noted as the starting gas is used, the temperature of the canister decreases, causing the pressure to drop. If the STE does not start in the first few attempts, it may be beneficial to let the starting gas canister return to room temperature prior to subsequent start-up attempts.

Diffuser Modification.

The diffuser used in the ITB configuration was originally designed by Conrad [28] using a diffuser design code provided by David Burrus of Innovative Scientific Solutions Incorporated (ISSI). The original diffuser design is shown in Figure 45 with the components labeled. The boundary conditions used for the design were an inlet mass flow of 0.45 kg/s at a temperature of 1023 K, and an exit total pressure just above atmospheric. The length of the diffuser was limited to 12.7 cm in order to minimize the weight of the ITB. Mass flow splits designed for the diffuser were determined from the literature [11, 17] and using CHEMKIN, a reaction modeling code. The flow splits designed to be tested were a 60/40, 70/30, and an 80/20 core flow to bypass flow configurations. The flow split ratios were based on the ratios of inlet areas for the core and diffuser flow paths. For each diffuser Middle Diameter (MD), the dimensions at the interface to the UCC front plate are kept constant, and only the forward MD dimensions are varied. The diffuser inlet core to bypass area ratios for the three diffuser flow splits are shown in Table 4. A comparison of the three MD designs are shown in Figure 46.

56

Table 4: Core/Bypass Area Ratio by Diffuser Flow Split

Diffuser Flow Split	Core Area (cm^2)	Bypass Area (cm^2)	Area Ratio
60/40	22.04	32.83	0.67
70/30	26.20	28.60	0.92
80/20	29.85	24.88	1.20
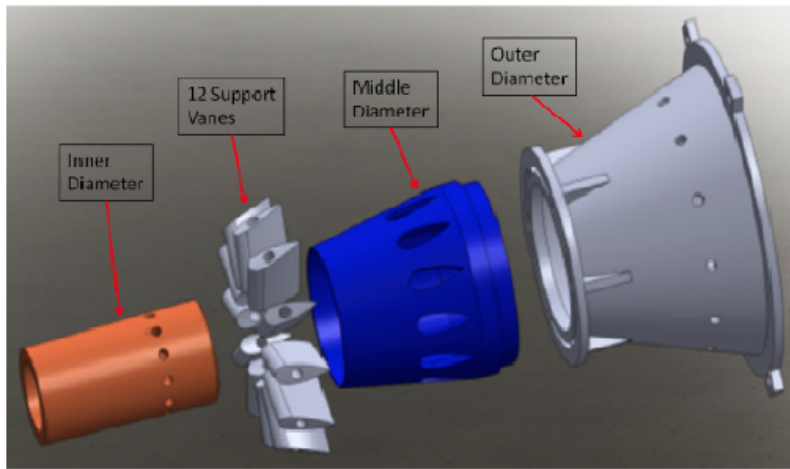
Figure 45: Original Diffuser Exploded View [28]

To experimentally verify the designed diffuser core to bypass mass flow splits, modifications needed to be made to the existing diffuser. The original diffuser did not allow for pressure or temperature measurements to be taken within the diffuser. An exploded view of the diffuser with parts modification is shown in Figure 47. The Outer Diameter (OD) was modified with the addition of nine 1/16 inch NPT measurement ports that can be used for either pressure or temperature measurements. Of the nine measurement ports, three ports were located just aft of the diffuser inlet and forward of the MD so inlet conditions can be measured. Six measurement ports are located near the exit of the diffuser OD. Three of the aft measurement ports can be used to take measurements within the diffuser bypass flow, and three can be used to take measurements within the

57
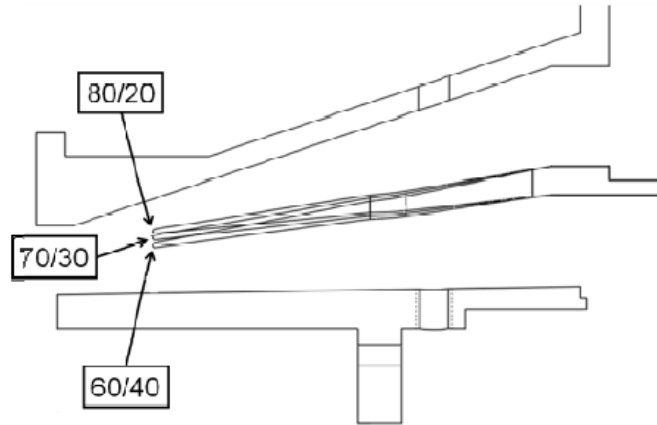
Figure 46: MD Comparison, 80/20, 70/30, 60/40 [28]

core flow. All three MD configurations were modified to include three 1/16 inch access ports aligned with three of the 1/16 inch NPT fitting on the OD. For this investigation, the diffuser was instrumented with two static pressure probes, and two total pressure probes using four of the six aft diffuser measurement ports. The pressure probes used were capable of measuring the total and static pressure in the core and bypass flows. The area at the location where the total pressure was measured is required to calculate the mass flow in each diffuser flow path. The areas used for the diffuser mass flow calculations were determined from the solid models shown in Figure 48. The point where the total pressure is measured, and therefore, the location at which the area should be determined, was 0.635 cm forward of the probe insertion point. Table 5 shows the areas used for each location where the mass flow was calculated.

For this experiment it is assumed the flow exiting the HPT rotor, simulated by the STE, has zero swirl entering the diffuser. The validity of this assumption is supported by the fact axial flow is desired at the exit of a gas turbine engine to maximize the potential thrust that can be achieved. Therefore, it is assumed the swirl in the exit flow of the STE is negligible. For this reason only the straight diffuser support vanes are used in this
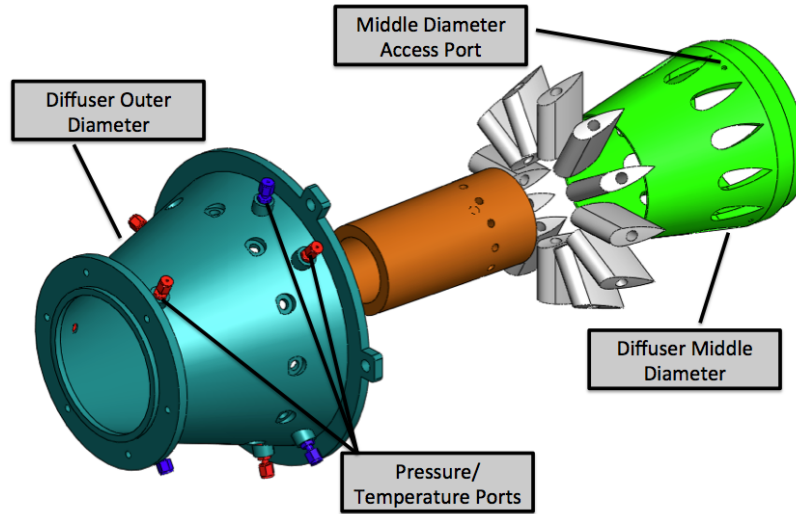
Figure 47: Modified Diffuser Exploded View
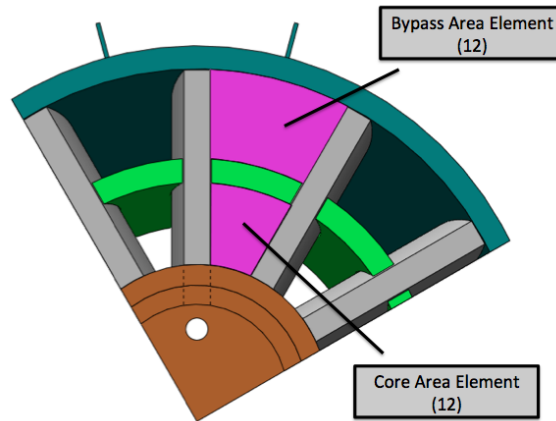
Figure 48: Diffuser Area Measurement Locations

experiment. The modified diffuser OD and the three modified MD configurations are shown in Figures 49(a) and 49(b) respectively.

Air Injection Panels.

For the ITB configuration, the air to the circumferential cavity of the UCC is supplied through the front plate with the use of three air injection panels. Figure 50 shows the air

Table 5: Area by Location

Diffuser Split	Location	Area Element (cm^2)	Total Area (cm^2)
	Inlet		77.07
60/40	Core	5.78	69.36
60/40	Bypass	2.75	33.00
70/30	Core	5.72	68.64
70/30	Bypass	2.80	33.60
80/20	Core	5.66	67.92
80/20	Bypass	2.85	34.20
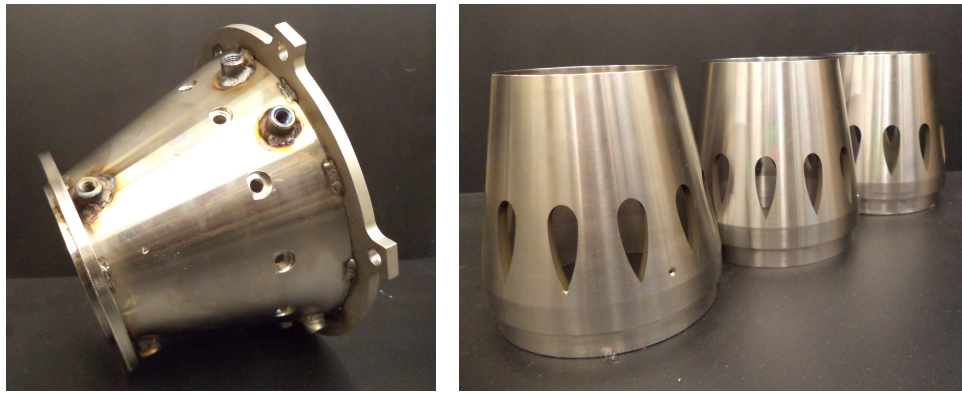
(a) Diffuser OD   (b) Three Diffuser MD Configurations

Figure 49: Modified Diffuser Components

injection panel machined from Hastelloy-X by the AFIT machine shop. The original air injection panel designed by Conrad [28] had 22 air injection holes. The decision was made to increase the injection hole diameter to match the diameter used by Wilson [29]. The increased hole diameter reduced the number of holes needed per panel to 20 to match the cavity flow rate of 1.08 kg/min tested by Wilson. The holes in the air injection panel are 0.45 cm in diameter, and the air is injected 30° from the axial direction.

Figure 50: Air Injection Panel

Three air injection panels are mounted to the UCC front panel as shown in Figure 51. The air injection panels are fed by the bypass flow of the diffuser and are designed to provide the necessary clockwise circumferential velocities required to achieve the desired g-loads in the circumferential cavity. The target g-loads for this configuration are between 1000-2000 g, which would match the g-loading achieved by Wilson [29] for the same air injection hole diameter.
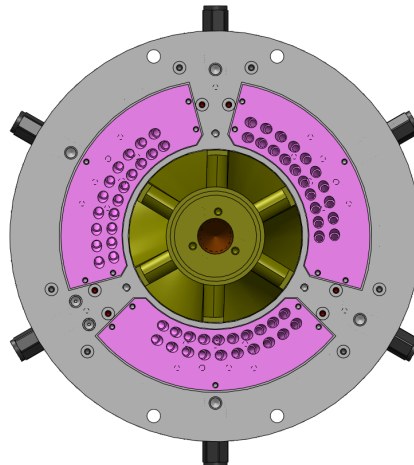
Figure 51: Air Injection Panels Mounted to UCC Front Plate

Circumferential Cavity.

The circumferential cavity used in the ITB configuration shares that same dimensions as the UCC circumferential cavity used in the work done by Wilson [11, 29]. The cavity has a diameter of 15.85 cm, and a cross sessional area of 6.45 cm^2. The combustion ring used by Wilson was replaced with a combustion ring without circumferential air injection holes. The fluid flow through the circumferential cavity is shown in Figure 52. Air enters the cavity through the air injection panel where it is swirled in a clockwise direction. Fuel is supplied through six 0.3 flow number fuel nozzles spaced 60° apart around the circumference of the cavity. As reactions occur, the heavier, unreacted, products remain in the cavity while reactions continue. The lighter combustion products migrate inward radially and exit the cavity through the center body and out the ITB exit.
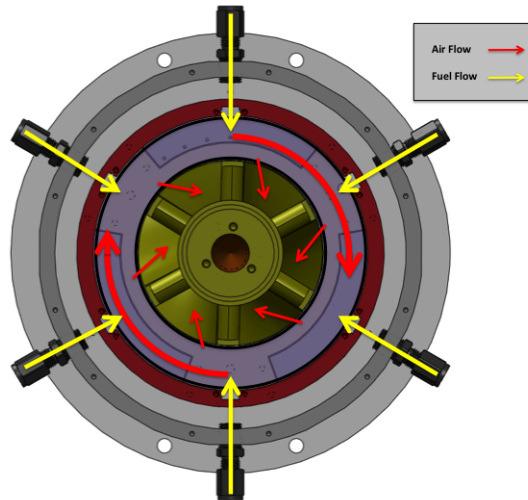
Figure 52: Fluid Flow Through Circumferential Cavity (Front View)

Center Body Design.

The intent of the ITB configuration is to act as a burner between the HPT and the LPT. In an effort to reduce weight, the ITB incorporates the LPT vane by taking zero degree swirl vitiated air from the HPT rotor, reheating the flow, and turning the flow ~70°

before feeding it to the LPT rotor. In order to turn the flow from 0° to 70°, a new center body design was necessary. The new center body built upon the Low Loss Center Body (LLCB) design used by Wilson [11, 29]. The original LLCB was designed to take in air at an angle of 30°, and turn the flow to exit at 70°. The new center body is a modification of the LLCB, where the forward section of the center body was modified to accept axial flow. The core and exit angle of the original LLCB was kept, but the vane sweep was modified to accept a 0° swirl flow. This new design is shown in Figure 53. The center body is 10.16 cm long and has an outer diameter of 10.8 cm. The inner diameter of the center body follows the profile designed by Wilson for the LLCB; a full discussion of that design can be found in reference [29]. The center body is mounted to the aft end of the diffuser, and is held in the ITB when the diffuser is mounted to the front plate.

(a) Front View   (b) Isometric View   (c) Side View
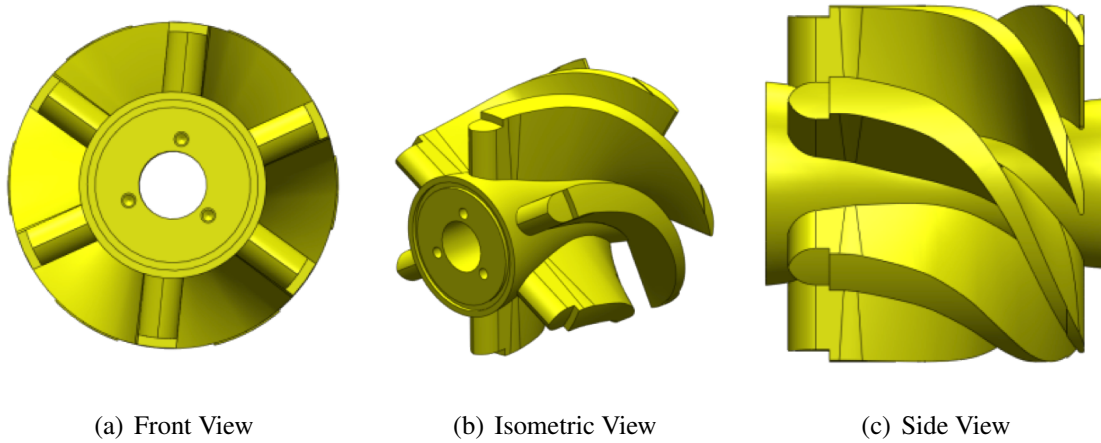
Figure 53: ITB Center Body

ITB Aft Section.

The ITB aft section consists of the back plate, instrumentation panel, blank panels, exhaust tube, instrument exit ring, and tail cone. The aft section of the ITB is shown in Figure 54. The rear instrumentation plate has seven 1/16 inch NPT instrumentation ports, and is used to measure static and total circumferential cavity pressures in addition to

cavity temperature. For this experiment, only one instrumentation panel is used to measure circumferential cavity total and static pressure and temperature. The instrumentation panel has a single static pressure probe, and total pressure probes placed at the 1/4 and 1/2 cavity span locations as measured from the back plate. The temperature of the cavity is measured with a thermocouple. These measurements are used to calculate g-loads in the cavity, and will be discussed later in this Chapter. Two blank insert panels are used to seal the two non-instrumented panels voids in the back plate. The instrumentation exit ring has 21 1/16 inch NPT instrumentation ports, and measures the exit conditions of the ITB including temperature and pressure. An ignition source is provided to the cavity through the back panel of the ITB using an ethylene and air mixture. The mixture is ignited by a Maxon 18075 spark igniter, which supplies a flame to ignite the fuel/air mixture in the circumferential cavity.
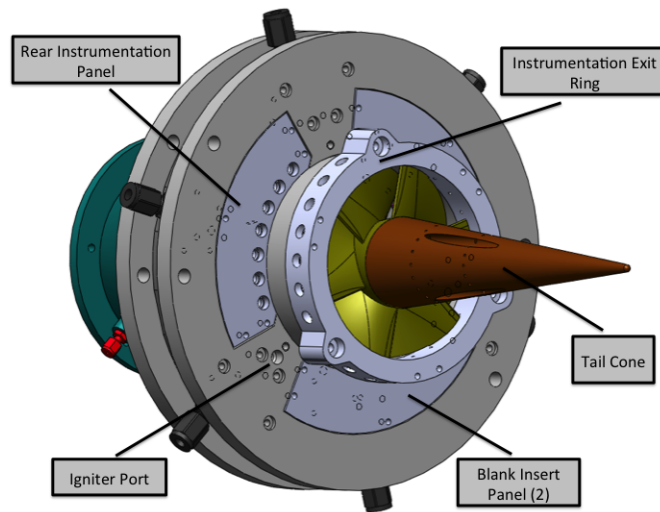
Figure 54: Aft View of ITB Configuration

Fuel System

JP-8 is supplied to the circumferential cavity during testing of the ITB configuration. Fuel is supplied to the ITB with an ISCO 1000D dual syringe pump, feed by a 19 liter stainless steel Alloy Products Corporation general purpose vessel. The pump is controlled using the ISCO Series D pump controller per manufacturer instructions [32]. The dual syringe pump is capable of providing a continuous flow up to 408 mL/min at a pressure of 2000 psi. Facility compressed air is supplied to the pump to facilitate solenoid activation. Figure 55 shows the ISCO pump and controller. Fuel is routed to the ITB through 0.25 inch stainless steel tubing, and filtered through a 0.5 micron Swagelok filter, atomized in the circumferential cavity by six 0.3 flow number fuel nozzles.

Figure 55: ISCO Pump and Controller [18]

Instrumentation

The instrumentation used for the experiments in this work are primary composed of pressure and temperature transducers with their associated electronics and LabVIEW VIs.

A thrust stand is also used to characterized the thrust of the STE used in the ITB experiments.

Thrust Stand.

The thrust stand consist of a 18 x 24 inch Thorlabs optical breadboard mounted on four Newway 2 inch air bushings. The air bushings are mounted on two 2 inch diameter, 3 ft machined steel. Facility air is supplied to the bushings at 80 psi to allow for smooth travel of the air bushings over the steel rods. An Interface SM-150 force transducer is mounted between the thrust stand chassis and the optical breadboard. A LabVIEW force transducer VI is used to collect force measured by the thrust stand. The thrust stand assembly can be seen in Figure 56. Calibration of the thrust stand is accomplished by calibrating the force transducer prior to installation on the thrust stand. The details of the full calibration procedure for the force transducer can be found in Appendix B.
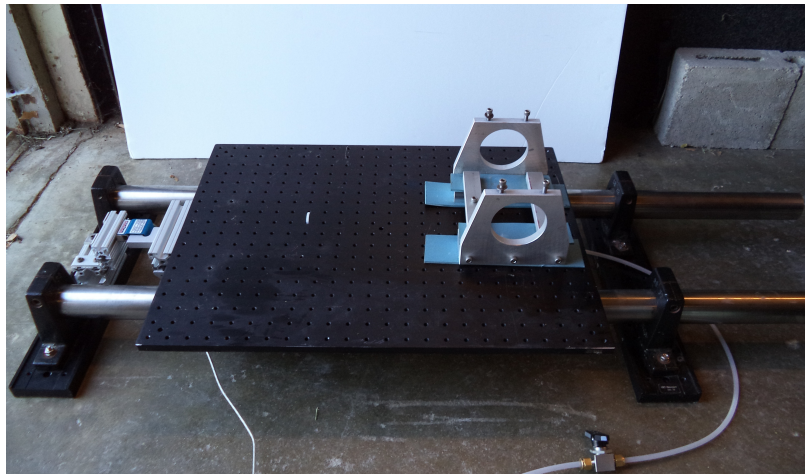
Figure 56: Thrust Stand

Temperature and Pressure.

Pressure measurements are made using a 64 channel ESP-HD pressure scanner connected to an Esterline DTC Initium acquisition system. Data collection is accomplished through a modified version of the manufacturer provided Esterline data

acquisition LabVIEW VI. The pressure data acquisition components are shown in Figure 57. The pressure measurement system outputs differential pressures and require the laboratory to be equipped with an Omega PX305-015AI pressure transducer to provide an absolute pressure measurement for comparison.

(a) ESP-HD Scanner   (b) Esterline DTC Initium [28]

Figure 57: Pressure Data Acquisition Components

Temperature data is collected using 1/16 inch K-type probe thermocouples. A thermocouple bank capable of accommodating the use of up to 48 thermocouples is monitored using a LabVIEW VI. The VI is controlled from the COAL lab control station. The thermocouple bank is shown in Figure 58.
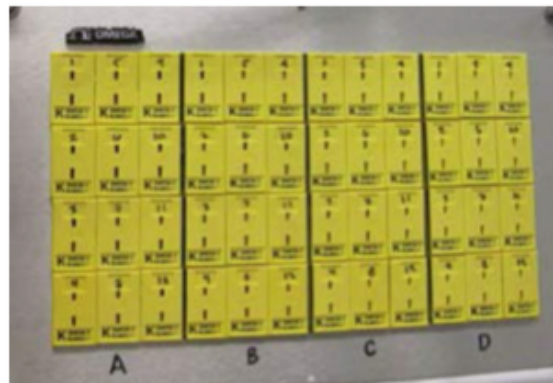
Figure 58: Thermocouple Bank

COAL Laboratory Updates

Several data collection improvements were needed to existing LabView VI software programs at the COAL lab control station, and new VIs needed to be developed to collect new data types. The RigControl VI, developed by Wilson, lacked the ability to write data to file for post processing. The VI was modified to include the needed write-to-file functionality. The LabView VI provided by Esterline for collecting pressure data from the DTC Initium pressure scanning system was also modified to include the same write-to-file functionality as the RigControl VI.

To measure the thrust produced by the JetCat P200 and the AFIT ITB an Interface SM-150 150 lbf load cell was used. No software existed to take measurements using such a force transducer. A Force Transducer VI was developed to read in the voltage from the force transducer, and convert the voltage to a force measurement. A pressure transducer was needed to monitor the absolute pressure in the COAL lab so the differential pressures provided by the 64 channel pressure scanner could be converted to absolute pressures. An Omega PX305-015AI pressure transducer, with a range from 0 to 15 psia, was used to measure the absolute pressure at the ITB. The ForceTransducer VI was modified to measure a 0 to 20 mA input amperage and convert it to units of psia.

ITB Integration Results

This section discusses the tests conducted and the results achieved for the experimental ITB integration study, with the objective of making progress towards integrating the AFIT UCC to function as an ITB. The experimental components of this work consist of the ITB diffuser performance study and thrust characterization of the JetCat P200. The goal of the ITB diffuser study was to verify the designed flow splits and to determine if the designs are capable of providing sufficient air flow to the circumferential cavity to results in g-loads between 1000-2000 g. The results of the numerical analysis consist of a thrust augmentation, and a Power Extraction (PX)

augmentation study of an ITB engine versus an afterburning engine. These studies seek to determine the most promising application of the ITB when used for engine performance augmentation. The numerical results of the effects of ITB pressure drop are also presented in this chapter. The pressure drop study seeks to explore the range of pressure drops an ITB can possess and still provide acceptable performance augmentation. A baseline measurement of thrust at various engine rpm settings will allow for a basis of comparison for future ITB work incorporating the use of the JetCat P200.

ITB Diffuser Performance Characterization.

The instrumented ITB configuration used for the experimental performance evaluation of the diffuser is shown in Figure 59. Temperatures and pressure at the inlet, diffuser core, diffuser bypass, and circumferential cavity are recorded at the control station. In addition to the measurements taken at the ITB configuration the inlet mass flow supplied by the mass flow meter is recorded. The ambient pressure at the ITB is recorded so the measured pressure differentials can be converted to absolute pressure measurements.
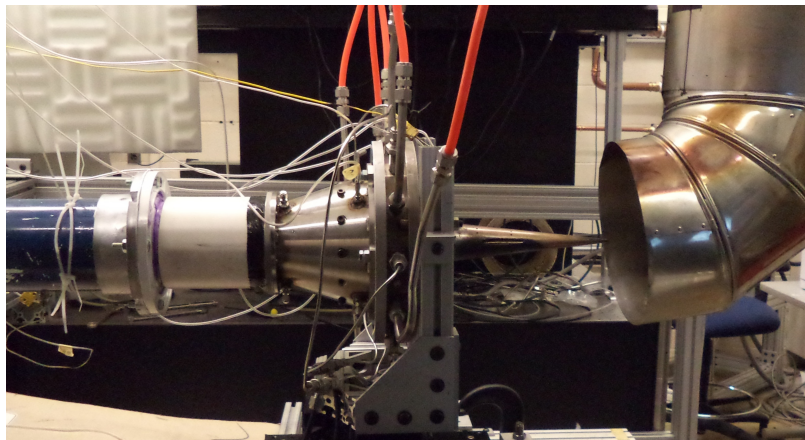
Figure 59: ITB Configuration with Compressed Air

With the pressures recorded at each location of interest in the ITB configuration, the Mach number can be calculated using Equation 5. Where P_t and P_s are the total and static pressures measures by the pressure probes. Since this experiment used ambient compressed air, the ratio of specific heats was chosen to be $\gamma = 1.4$.

$$M = \sqrt{\left[\left(\frac{P_t}{P_s}\right)^{\frac{\gamma-1}{\gamma}} - 1\right]\frac{2}{\gamma - 1}}$$

(5)

The Mach number is used to calculate the velocity at each location using Equation 6. Where T is the temperature measured by the thermocouple and the gas constant for air is selected to be $R = 287\frac{J}{kgK}$. At each location, the total pressure probes are configured to be aligned with the velocity vector at that location. In the case of the circumferential cavity, the total pressure probes are oriented in line with the tangential velocity vector in the cavity.

$$V = M\sqrt{\gamma RT}$$

(6)

The density for air can be calculated at each location using Equation 7. The temperature used for the density calculated in the inlet and diffuser core and bypass flows is measured in the inlet duct.

$$\rho = \frac{P_s}{RT}$$

(7)

The calculated velocity and density in the inlet and diffuser are used to compute the mass flows at each location using Equation 8, where A is the total area at each location tabulated in Table 5.

$$\dot{m} = \rho A V$$

(8)

The cavity g-loading can be calculated using Equation 9, the radius where the measurements were taken is $r = 6.68$ cm and $g_o = 9.81\ \frac{m}{s^2}$.

$$g = \frac{V^2}{rg_o} \tag{9}$$

The ITB diffuser study was performed with the diffuser mounted to the front plate of the UCC as shown in Figure 59. The center body design discussed previously in this chapter was not manufactured due to fiscal constraints, and was not used in the experiment. The low loss center body designed by Wilson [29] was used in its place to provide a pressure drop across the diffuser core flow path. Table 6 list the diffuser test cases and associated mass flows and corresponding inlet mach numbers. The dedicated compressed air source was specified to provide a constant mass flow of 0.6 kg/s, and this condition is defined as 100% mass flow. In application, the compressor was not able to produce a constant mass flow above a value of ~70% mass flow. Testing was conducted at mass flow percentages of 30%, 40%, and 50% with mass flow rates of 0.18 kg/s, 0.24 kg/s, and 0.30 kg/s respectively. The 30% and 40% mass flow rates were able to provide adequate time at the desired condition after temperature and mass flow rate stabilization of the ITB configuration. The 50% mass flow rate was used with the 80/20 diffuser flow split only to see if a third mass flow percentage would yield a different trend in the data.

Table 6: Diffuser Test Cases

Test Case	Flow Split	Air Mass Flow (kg/s)	Inlet M
A	60/40	0.18	0.055
B	60/40	0.24	0.074
C	70/30	0.18	0.054
D	70/30	0.24	0.073
E	80/20	0.18	0.054
F	80/20	0.24	0.072
G	80/20	0.30	0.084

The desired results of this experiment would be to see the mass flows for each diffuser test case flow split match the designed diffuser flow split. This was not the case for most of the diffuser test cases. Table 7 shows the calculated inlet, core, and bypass mass flows as well as the diffuser flow splits and cavity g-loading for all diffuser test cases. For all of the 60/40 and 70/30 diffuser test cases, the calculated flow splits remained at about a ratio of 70/30. Each diffuser test case showed similar core mass flows at matching inlet mass flow conditions, which may demonstrate that the mass flow split is a function of the pressure losses in each flow path and not a function of diffuser inlet area ratio. The best match to the designed mass flow split was Test Case C in which a flow split of 70.2/29.8 was observed.

During data collection for all experiments the total pressure and the static pressure in the bypass stream fluctuated significantly. This fluctuation may contribute to the failure of the combined core and bypass mass flow to match the calculated inlet mass flow. When the bypass stream data was studied on a point by point basis, it showed there existed several instances where the static pressure was greater than the total pressure. The total and static pressures for each diffuser test case are presented in Figure 60. Bypass mass flow or diffuser flow splits could not be calculated for all 80/20 diffuser test cases due to an adverse total pressure to static pressure ratio. The adverse total to static pressure ratio does not allow the Mach number to be calculated, which is needed to perform mass flow calculations. The g-loads generated by each diffuser test case are significantly lower than expected. Using the AFIT UCC configuration with similar bulk air mass flows, g-loads from 1000-2000 g's were observed. The common flow source diffuser configuration did not approach the high g-load values observed during previous work with AFIT UCC [29]. The data in Figure 60 references to transducer numbers which are defined in Table 8.

To investigate the significance of the bypass stream total and static pressure fluctuation, a t-test was performed on each pair of total and static pressures for each test

Table 7: Diffuser Mass Flow Comparison

	Diffuser Test Case						
	A	B	C	D	E	F	G
Inlet $\dot{m}$ kg/s	0.184	0.250	0.178	0.250	0.181	0.248	0.291
Core $\dot{m}$ kg/s	0.168	0.217	0.169	0.216	0.167	0.218	0.258
Bypass $\dot{m}$ kg/s	0.070	0.111	0.072	0.064	N/A	N/A	N/A
Core Flow (%)	70.4	66.1	70.2	77.2	N/A	N/A	N/A
Bypass Flow (%)	29.6	33.9	29.8	22.8	N/A	N/A	N/A
Cavity G-load	454	738	411	642	298	500	719

case. A two sample t-test is a measure of the difference between two independent sets of data. In this case, it is used to determine if there is a significant statistical difference between the total and static pressure measurements. The t-test does this by testing to see if the null hypothesis is true. The null hypothesis states there is no statistical significance between the means of two data sets. The t-test determined the null hypothesis could not be discounted for the bypass stream in cases C and D. The associated p-values for the bypass stream of Cases C and D are 0.0695 and 0.3344 respectively. P-values are used to determine wether or not to ignore the null hypothesis and the null hypothesis is usually ignored for $p < 0.05$. This means that even though values for the bypass stream mass flow and flow splits were calculated for cases C and D they may not be accurate, and should be ignored. This also means that the adverse total pressure to static pressure ratio for Cases E, F and G may accurately represent what is happening in the experiment. This leaves the 60/40 flow split diffuser design as the only diffuser configuration that does not experience an adverse total to static pressure ratio.
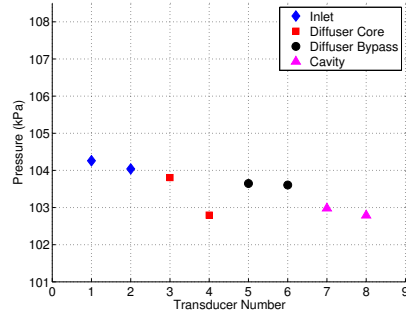
(a) Case A
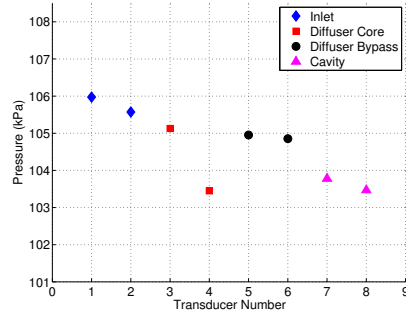
(b) Case B
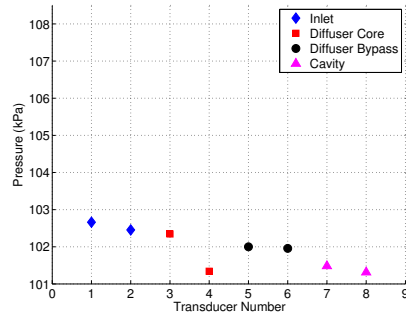
(c) Case C
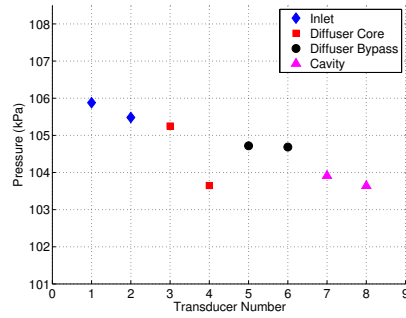
(d) Case D
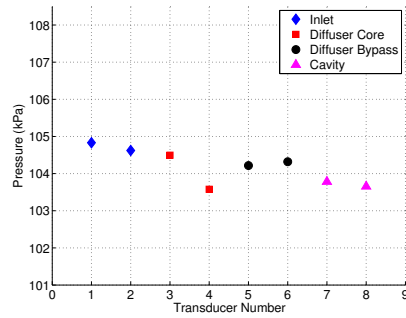
(e) Case E
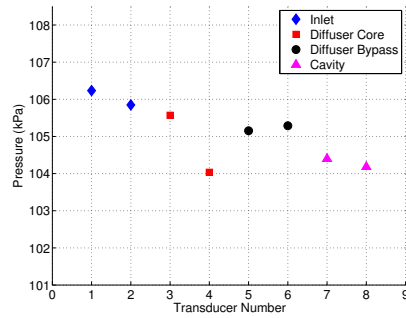
(f) Case F
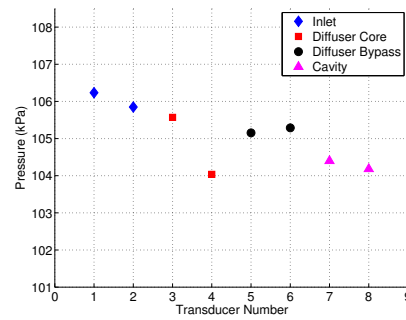
(g) Case G

Figure 60: Total and Static Pressure Data by Diffuser Test Case

Table 8: Transducer Numbers

Transducer	Measurement
1	Inlet P_t
2	Inlet P_s
3	Core P_t
4	Core P_s
5	Bypass P_t
6	Bypass P_s
7	Averaged Cavity P_t
8	Cavity P_s

Another method used to determine the performance of the diffuser designs was to compare the pressure drops (dP/qP) across the core and bypass flow paths, and determine a mixing ratio (R_{mix}) between the two paths. Table 9 shows the results for the pressure drop investigation. The circumferential cavity of the ITB is a mixer that combines a core and a bypass stream. The mixer in a mixed stream turbofan engine is designed so the R_{mix} ratio is always greater than unity. Values less than unity can be problematic because the bypass flow is at a lower total pressure than the core flow which can potentially cause flow reversal in the bypass duct thereby stalling the HPT. If an R_{mix} value greater than unity is desirable of a conventional mixer, then it should also be a desirable property of the ITB diffuser. Table 9 shows every diffuser test case suffers from an R_{mix} value less than unity with, cases E, F, and G having the lowest ratios. This phenomena may help to explain the significant fluctuations in diffuser bypass total and static pressures, as well as the consistently higher static pressures in cases E, F, and G. The fluctuations and higher static pressure values are most likely instances of flow reversal in the bypass stream of the diffuser. This reduces the velocity of the flow into the total pressure probe, which is facing

towards the diffuser inlet, causing the static pressure to appear greater than the total
pressure.

Table 9: Diffuser Pressure Drop Comparison

	Diffuser Test Case						
	A	B	C	D	E	F	G
Inlet P_t	104.26	105.97	102.66	105.88	104.83	106.23	107.65
Core P_t	103.81	105.13	102.35	105.25	104.50	105.57	106.68
Bypass P_t	103.65	104.95	102.00	104.72	104.22	105.15	103.65
Core dP/qP	0.4343	0.7973	0.3074	0.5928	0.3195	0.6240	0.8976
Bypass dP/qP	0.5884	0.9633	0.6454	1.0958	0.5852	1.0159	3.7166
R_{mix}	0.9985	0.9983	0.9966	0.9949	0.9973	0.9961	0.9716

STE Thrust Characterization.

Thrust data was collected on the JetCat P200 to determine how the baseline thrust
output compared to the manufacturer's rating. The thrust testing configuration is shown in
Figure 10. The thrust measurement experiment was conducted in the COAL lab. The
thrust stand was placed at the exit door on the North wall of the lab, and the JetCat P200
was mounted with the exhaust facing out though the open door. As mentioned earlier, the
JetCat P200 can be controlled either by the JetCat GSU or from the LabVIEW VI at the
COAL lab control station. For this experiment the GSU was used to control the STE
during set up verification of the experiment. During actual testing of the JetCat P200 the
STE was controlled from the LabVIEW VI. Controlling the STE from the control station
allowed for the force measurements to be easily recorded using the Force Transducer VI.
The JP-8 fuel tank was filled with ~2.8 kg of fuel prior to testing and a full canister of
MSR IsoPro starting gas was used. Since the JetCat P200 consumes ~0.45 kg/min [30] of
fuel at full power the testing duration was less than five minutes to ensure that the fuel

supply was not exhausted. Table 10 shows the test matrix used and the priority of test points that was established. The entire test matrix was accomplished in one continuous session of STE thrust testing.
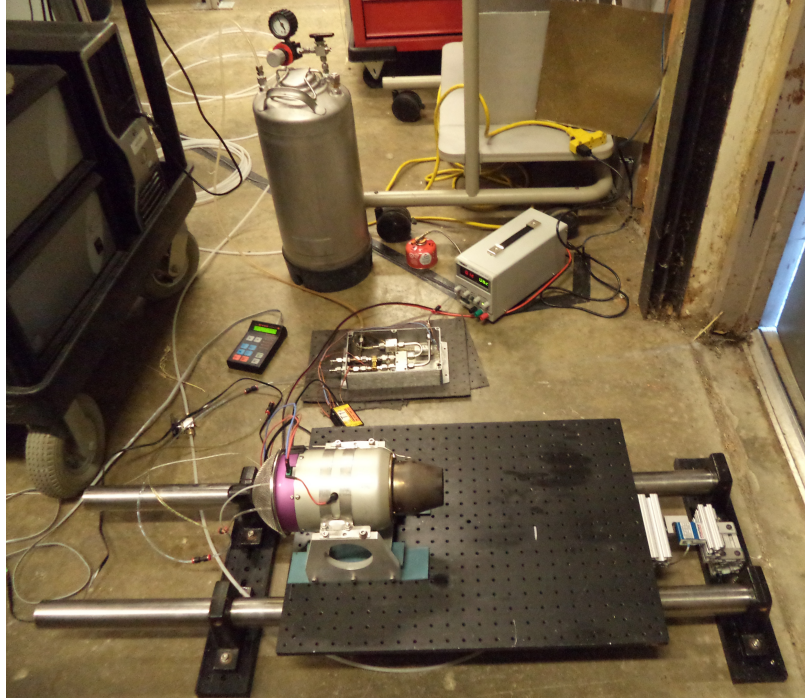
Figure 61: JetCat P200 on Thrust Stand

The results of the experiment are shown in Figure 62. The values for engine rpm vary from 33000 at idle to a maximum of 112000 at full power. The values recorded for engine rpm during the experiment are for the specified rpm and not the actual engine rpm. The software used is not configured to record actual engine rpm and is only capable of recording the specified rpm. Once the engine stabilized at the specified rpm value, the actual rpm value returned from the JetCat Engine Control Unit (ECU) varied slightly. This variation in actual engine rpm can be seen as a variation in the force measured in Figure 62. Figure 62 shows the average maximum thrust at full power was ~200 N, which is comparable to the manufacturer set point of 205 N, stored in the JetCat P200 ECU. A

Table 10: STE Thrust Test Matrix

Test Point	Specified Engine RPM
1	33000
2	112000
3	73000
4	103000
5	43000
6	93000
7	53000
8	83000
9	63000

second order polynomial line was fitted to the data to estimate the thrust produced for any engine rpm setting. The result of the second order polynomial fit line is shown in Equation 10, which is used to calculate thrust values by rpm with a standard deviation of 6.1 N. The values for the thrust, F, in Equation 10 are in Newtons.

$$F = 0.0317(rpm)^2 - 2.1963(rpm) + 50.2375 \qquad (10)$$

Figure 62: JetCat P200 Thrust vs RPM

V.   Conclusions and Recommendations

The use of an ITB has not been previously explored to determine the applications best suited to this technology. The objectives of this work are to identify the engine applications where the ITB provides better engine performance, in terms of fuel efficiency, compared to that of an afterburner, and to make progress towards integrating the AFIT UCC into an ITB configuration. A numerical analysis was performed using NPSS to determine the best 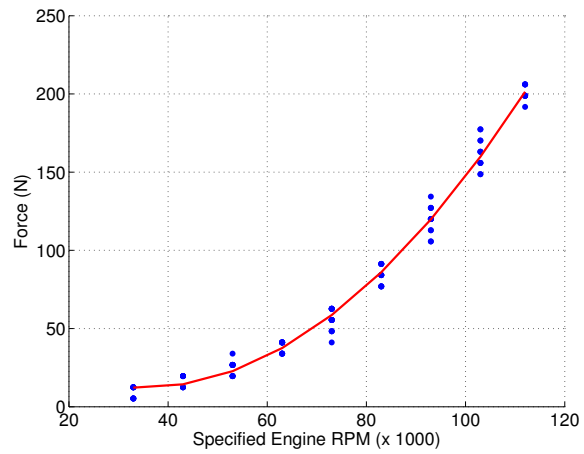candidate application for the ITB engine cycle. The effect of ITB pressure drop was investigated to determine a range of pressure drops the ITB must achieve in order to provide better engine performance augmentation than an afterburner. The performance of the ITB common flow source diffuser had been investigated to determine it's ability to provide air flow to the core and circumferential cavity of the AFIT ITB. Thrust testing has been conducted on the ITB vitiated air source, a JetCat P200, to establish it's baseline performance. The baseline thrust of the vitiated air source provides a basis of performance comparison for the ITB configuration. The conclusions drawn from the the results of these investigations, as well as suggestions for future follow on work are presented in the following section.

Numerical Conclusions

The ITB engine yielded superior results in the thrust augmentation study. The ITB engine demonstrated a significantly smaller increase in TSFC compared to the afterburning engine. The heat addition between the HPT and LPT did, however, result in significantly reduced fan efficiency and HPC stall margin encroachment for ITB model. Therefore, the ITB may not be the best candidate for thrust augmentation in a mixed stream turbofan engine. The problems associated with burring between the turbines during thrust augmentation may be resolved if the ITB is used with a separate stream

turbofan engine and a geared fan. This would reduce the problems associated with fan overspeed negatively affecting the ITB engine model.

Next, the engine models were compared when PX augmentation was required. Additional shaft power requirements potentially arise from additional electrical loads required by an aircraft. The models require increased shaft power while maintaining constant thrust at military power. In this investigation, the ITB engine had a similar TSFC trend as that achieved for thrust augmentation, but without the negative effects. These results are attributed to the energy added to the system by the ITB extracted as shaft power. This significantly minimizes the fan overspeed condition, and reduces the core stream total pressure at the mixer. This study showed the ITB is better applied to instances where increased shaft power is required without using additional thrust.

Lastly, the effects of ITB pressure drop were investigated to determine the range of values necessary to achieve the desired benefits of using an ITB equipped engine. The pressure drop was varied for the case of PX augmentation. ITB pressure drops are expected to be in the range os 0.03 to 0.05, and for this range, the study showed the ITB provides superior results, in terms of fuel efficiency, to an afterburning engine.

ITB Integration Conclusions

An experimental determination of ITB diffuser performance was conducted on three separate diffuser configurations. The configurations tested core to bypass air flow splits of 60/40, 70/30, and 80/20, based on diffuser inlet area percentages. All three diffuser configurations were tested at mass flow rates of 0.18 kg/s and 0.24 kg/s; and the 80/20 flow split was also tested at a flow rate of 0.30 kg/s. Total and static pressures were recorded at the inlet, diffuser core, diffuser bypass, and circumferential cavity. Temperatures were recorded at the inlet and in the cavity. From the data collected, mass flows could be calculated for the diffuser core and bypass streams. All three diffuser configurations generated mass flow splits of ~70/30, which was not originally intended of

Conrad's designs. All diffuser configurations demonstrated R_{mix} values less than unity. These results imply instances of reversed flow may be present in the bypass steam of the diffuser. The results of the statistical t-test conducted on the total and static pressure data for the diffuser bypass show that occurrence of flow reversal may be more prevalent in the 70/30 and 80/20 diffuser configurations than in the 60/40 configuration. The ability to calculate g-loading in the circumferential cavity make it difficult to draw a definitive conclusion of the flow properties in the diffuser bypass stream. While the g-load may be caused by the flow through the air injection panels fed by the diffuser bypass, it may also be a product of the core fed air flowing into the cavity. The 60/40 diffuser configuration was the best choice for incorporation into the ITB by exhibiting greater total pressure than static pressure in the bypass stream, and an R_{mix} value of ~0.998. The 60/40 diffuser configuration will require the least modifications to increase the R_{mix} to a value greater than unity.

The JetCat P200 STE is the proposed vitiated air source to be used for future research of the AFIT ITB. An experiment was performed to determine the thrust performance of the JetCat P200 that can later be used for ITB performance comparison. The STE was mounted on a thrust stand and force measurements were taken at various engine rpm settings. A thrust to rpm curve was determined for the STE for a range of engine rpm values from 33000 (idle) to 112000 (full power). The maximum thrust was determined to be approximately 200 N, which was consistent with the manufacturer specified value for thrust at full power.

Recommendations for Future Work

Progress has been made toward understanding the applications best suited to an ITB cycle, and integrating the AFIT UCC to an ITB configuration. Further investigations and improvements can be conducted to continue to advance the study of the AFIT ITB. A flow visualization study should be conducted in the cavity to verify if flow reversal truly exist

within the bypass stream of the diffuser and to determine if the g loads calculated in the cavity are caused by a desirable circumferential flow in the cavity. The STE should also be run in the ITB configuration to ensure that its operation is not significantly affected by the exit conditions encountered at the diffuser. These test should be conducted prior additional fuel supplied to the circumferential cavity.

The models constructed using NPSS can be expanded upon to include additional studies into the use of the ITB in an actual engine cycle. A comparison should be done with the existing models over an entire mission profile to determine any overall mission benefits that can be provided by the ITB. A less complex model could also be developed to simulate the JetCat P200. This would provide a baseline model that could be expanded upon as research continues into the AFIT ITB.

Appendix A: JetCat P200 Operating Procedures with LabVIEW VI

Operating the JetCat P200 can be accomplished using the LabVIEW VI provided by AFRL. This simplified version of the AFRL operating procedures adjusted for use in the COAL lab.

JetCat P200 Starting Procedures

1. Make all necessary fuel/electrical connections per manufacturer instructions[31]

2. Turn on JetCat starting gas supply (MSR IsoPro)

3. Turn on JetCat JP-8 fuel supply

4. Turn on JetCat Power

5. Verify the ECU is powered by checking the GSU

6. Start the VI

7. Set COM channel to COM 3

8. Set Baud Rate to 9600

9. Press Start

JetCat P200 Power Down Procedures

1. Press Shutdown

2. Allow ECU to run the cool down sequence

3. Turn off JetCat power

4. Turn off starting gas and JP-8 supplies

Appendix B: Force Transducer Calibration

The model of force transducer chosen for this research is the Interface SM-150. This transducer has a range from 0 to 150 lbf. The transducer was mounted vertically as seen in figure (setup). A constant 10 VDC was supplied to the transducer from a TDK-Lambda 0-36 VDC power supply routed through an AFIT designed voltage regulator board. The transducer returns a signal voltage to a National Instruments NI 9205 analog input module which is read by a dedicated LabVIEW VI that converts the signal voltage to a force measurement. A small cord was attached to the measurement end of the transducer and weights were hung from the cord using a weight hanging plate. The weight hanging plate weighs 2 lb. Weights were loaded on the plate and loads from 0 to 89 lbf were applied to the transducer and the signal voltage and weight applied were recorded. The data was then post processed to verify that the calibration curve was linear and to determine the coefficients needed to convert from a signal voltage to lbf and N value. Figure 63 shows the calibration curve and the linear regression line fit to the data, and Equation 11 shows the calibration equation where V is the transducer signal voltage. The calibration constants were determined to be a slope of 4909.8 and y-intercept of 3.3566. The transducer standard deviation was calculated to be 1.22 N. Figure 64 shows the force transducer calibration setup.

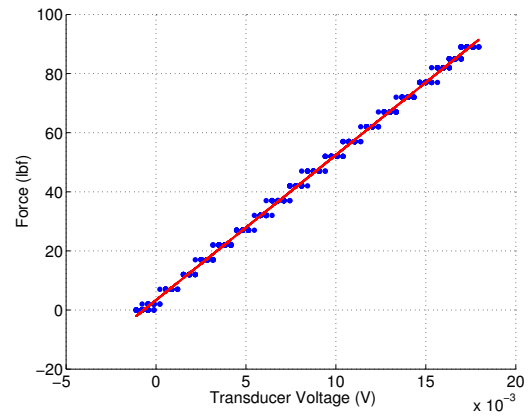$$F = 4909.8(V) + 3.3566 \qquad (11)$$

Figure 63: Force Transducer Calibration Curve

Figure 64: Force Transducer Calibration Setup

Bibliography

[1] Miranda, J. L., Polanka, M. D., and Simmons, R. J., "The Use of an Ultra-Compact Combustor as an Inter-Turbine Burner for Improved Engine Performance," 52nd *Aerospace Sciences Meeting*, AIAA 2014-0458, 2014.

[2] Bohan, B. T. and Polanka, M. D., "Analysis of Flow Migration in an Ultra-Compact Combustor," *Journal of Engineering for Gas Turbines and Power*, Vol. 135, No. 5, 2013, pp. 051502 1–11.

[3] Crane, R. I., "A Critical Analysis of the Thermodynamic Advantages of Reheat in Gas Turbines," *Proceedings of the Institution of Mechanical Engineers, Part A: Journal of Power and Energy*, Vol. 212, No. 2, 1998, pp. 81–87.

[4] Zelina, J., Shouse, D., and Hancock, R., "Ultra-Compact Combustors for Enhanced Gas Turbine Engines," *Proceedings of ASME Turbo Expo 2004*, GT2004-53155, 2004.

[5] Lewis, G. D., "Centrifugal-Force Effects on Combustion," *Symposium (International) on Combustion*, Vol. 14, No. 1, 1973, pp. 413–419.

[6] Zelina, J., Sturgess, G. J., and Shouse, D. T., "The Behavior of an Ultra-Compact Combustor (UCC) Based on Centrifugally-Enhanced Turbulent Burning Rates," 40th *AIAA/ASME/SAE/ASEE Joint Propulsion Conference and Exhibit*, AIAA 2004-3541, 2004.

[7] Anthenien, R. A., Mantz, R. A., Roquemore, W. M., and Sturgess, G. J., "Experimental Results for a Novel, High Swirl, Ultra Compact Combustor for Gas Turbine Engines," *2nd Joint Meeting of the US Sections of the Combustion Institute*, 2001.

[8] Yonezawa, Y., Toh, H., Goto, S., and Obata, M., "Development of the Jet-Swirl High Loading Combustor," 26th *AIAA/SAE/ASME/ASEE Joint Propulsion Conference*, AIAA-90-2451, 1990.

[9] Quaale, R. J., Anthenien, R. A., Zelina, J., and Ehert, J., "Flow Measurements Within a High Swirl Ultra Compact Combustor for Gas Turbine Engines," *XVI International Symposium on Air Breathing Engines*, ISABE-2003-1141, 2003.

[10] Blunck, D., Shouse, D., Neuroth, C., Battelle, R., Lynch, A., Sekar, B., Zelina, J., Erdmann, T., Burrus, D., and Howard, R., "Experimental and Computational Studies of an Ultra-Compact Combustor," *ASME Turbo Expo 2013: Turbine Technical Conference and Exposition*, GT2013-94372, 2013.

[11] Wilson, J. D., Conrad, M., and Polanka, M. D., "Flame Structure Effects at High G-Loading," *49th AIAA/ASME/SAE/ASEE Joint Propulsion Conference*, AIAA 2013-3712, 2013.

[12] Ciani, A., Eroglu, A., Guthe, F., and Paikert, B., "Full Scale Atmospheric Tests of Sequential Combustion," *Proceedings of ASME Turbo Expo: Power for Land, Sea and Air*, GT2010-22891, 2010.

[13] Vogeler, K., "Potential of Sequential Combustion for High Bypass Jet Engines," *ASME Turbo Expo 1998*, ASME 98-GT-311, 1998.

[14] Liu, F. and Sirignano, W. A., "Turbojet and Turbofan Engine Performance Increases Through Turbine Burners," *Journal of Propulsion and Power*, Vol. 17, No. 3, 2001, pp. 695–705.

[15] Liew, K. H., Urip, E., Yang, S. L., Mattingly, J. D., and Marek, C. J., "Performance Cycle Analysis of Turbofan Engine with Interstage Turbine Burner," *Journal of Propulsion and Power*, Vol. 22, No. 2, 2006, pp. 411–416.

[16] Zelina, J., Shouse, D., Stutrud, J., Sturgess, G., and Roquemore, W., "Exploration of Compact Combustors for Reheat Cycle Aero Engine Applications," *51st ASME International Gas Turbine and Aeroengine Congress and Exposition*, GT2006-90179, 2006.

[17] Spytek, C. J., "Application of an Inter-Turbine Burner Using Core Driven Vitiated Air in a Gas Turbine Engine," *ASME Turbo Expo 2012: Turbine Technical Conference and Exposition*, GT2012-69333, 2012, pp. 1017–1028.

[18] Conrad, M. M., Wilson, J. D., and Polanka, M. D., "Integration Issues of an Ultra-Compact Combustor to a Jet Turbine Engine," *49th AIAA/ASME/SAE/ASEE Joint Propulsion Conference*, AIAA 2013-3711, 2013.

[19] Gomes, K. J., Masiulaniec, K. C., and Afjeh, A. A., "Performance, Usage, and Turbofan Transient Simulation Comparisons Between Three Commercial Simulation Tools," *Journal of Aircraft*, Vol. 46, No. 2, 2009, pp. 699–704.

[20] Lytle, J. K., "The Numerical Propulsion System Simulation: An Overview," *CAS 2000 Workshop/The Ames Research Center*, NASA/TM-2000-209915, 2000.

[21] Huffman, B. C., Lavelle, T. M., and Owen, A. K., "An NPSS Model of a Proposed Altitude Test Facility," *49th AIAA Aerospace Sciences Meeting including the New Horizons Forum and Aerospace Exposition*, AIAA 2011-312, 2011.

[22] Jones, S. M., "Steady-State Modeling of Gas Turbine Engines Using The Numerical Propulsion System Simulation Code," *Proceedings of ASME Turbo Expo 2010: Power for Land, Sea and Air*, GT2010-22350, 2010.

[23] Daniele, C. J., Krosel, S. M., Szuch, J. R., and Westerkamp, E., *Digital Computer Program for Generating Dynamic Turbofan Engine Models (DIGTEM)*, NASA Technical Memorandum 83446, 1983.

[24] Corbett, M. and Wolff, M., "Modeling Transient Effects of a Double Bypass Engine," 8th *Annual International Energy Conversion Engineering Conference*, AIAA 2010-7090, 2010.

[25] Simmons, R., "Design and Control of a Variable Geometry Turbofan with an Independently Modulated Third Stream," Ph.D. Dissertation, Aerospace Engineering Department, The Ohio State University, 2009.

[26] Kestner, B., Nam, T., Flett, A., Wilson, J., and Mavris, D., "Integrated Engine and Aircraft Mission Performance Analysis Using NPSS," 50th *AIAA Aerospace Sciences Meeting including the New Horizons Forum and Aerospace Exposition*, AIAA 2012-841, 2012.

[27] Mattingly, J. D., *Elements of Propulsion, Second Edition*, Virginia: American Institute of Aeronautics and Astronautics, 2006.

[28] Conrad, M. M., "Integration of an Inter Turbine Burner to a Jet Turbine Engine," MS thesis, Department of Aeronautics and Astronautics, Air Force Institute of Technology (AU), Wright-Patterson AFB, OH, March 2013.

[29] Wilson, J., "Characterizing G-loading, Swirl Direction, and Rayleigh Losses in an Ultra Compact Combustor," MS thesis, Department of Aeronautical and Astronautical Engineering, Air Force Institute of Technology (AU), Wright-Patterson AFB, OH, June 2013.

[30] Baranski, J., Hoke, J., Litke, P., and Schauer, F., "Preliminary Characterization of Bio-fuels using a Small Scale Gas Turbine Engine," 49th *AIAA Aerospace Sciences Meeting including the New Horizons Forum and Aerospace Exposition*, AIAA 2011-694, 2011.

[31] JetCat USA, *Instruction Manual V6.0 ECU*, Paso Robles, CA, 2008.

[32] TELEDYNE ISCO, *D-Series Pumps Installation and Operation Guide*, Lincoln, NE, 2012.

REPORT DOCUMENTATION PAGE

Form Approved
OMB No. 0704–0188

The public reporting burden for this collection of information is estimated to average 1 hour per response, including the time for reviewing instructions, searching existing data sources, gathering and maintaining the data needed, and completing and reviewing the collection of information. Send comments regarding this burden estimate or any other aspect of this collection of information, including suggestions for reducing this burden to Department of Defense, Washington Headquarters Services, Directorate for Information Operations and Reports (0704–0188), 1215 Jefferson Davis Highway, Suite 1204, Arlington, VA 22202–4302. Respondents should be aware that notwithstanding any other provision of law, no person shall be subject to any penalty for failing to comply with a collection of information if it does not display a currently valid OMB control number. **PLEASE DO NOT RETURN YOUR FORM TO THE ABOVE ADDRESS.**

1. REPORT DATE *(DD–MM–YYYY)*	2. REPORT TYPE	3. DATES COVERED *(From — To)*
27–03–2014	Master's Thesis	Sep 2012–Mar 2014

4. TITLE AND SUBTITLE

The Use of an Ultra-Compact Combustor as an Inter-Turbine Burner for Improved Engine Performance

5a. CONTRACT NUMBER

5b. GRANT NUMBER

5c. PROGRAM ELEMENT NUMBER

6. AUTHOR(S)

Miranda Jr., Jose L., Captain, USAF

5d. PROJECT NUMBER

5e. TASK NUMBER

5f. WORK UNIT NUMBER

7. PERFORMING ORGANIZATION NAME(S) AND ADDRESS(ES)

Air Force Institute of Technology
Graduate School of Engineering and Management (AFIT/EN)
2950 Hobson Way
WPAFB, OH 45433-7765

8. PERFORMING ORGANIZATION REPORT NUMBER

AFIT-ENY-14-M-38

9. SPONSORING / MONITORING AGENCY NAME(S) AND ADDRESS(ES)

Air Force Office of Scientific Research
Dr. Chiping Li
875 N Randolph St, Ste 325 Rm 3112
Arlington AFB VA, 22203
chiping.li@us.af.mil

10. SPONSOR/MONITOR'S ACRONYM(S)

AFOSR

11. SPONSOR/MONITOR'S REPORT NUMBER(S)

12. DISTRIBUTION / AVAILABILITY STATEMENT

DISTRIBUTION STATEMENT A:
APPROVED FOR PUBLIC RELEASE; DISTRIBUTION UNLIMITED

13. SUPPLEMENTARY NOTES

This material is declared a work of the U.S. Government and is not subject to copyright protection in the United States.

14. ABSTRACT

An Inter-Turbine Burner (ITB) represents a novel mechanism for generating additional work from a gas turbine engine in applications where an afterburner would typically be used. An ITB can achieve higher thermal efficiencies over a typical afterburner while also generating shaft work versus only additional thrust.

In an effort to investigate the potential applications for the ITB, a numerical engine cycle comparison was made between the ITB cycle and a conventional afterburning cycle using the Numerical Propulsion System Simulation (NPSS). In the case of thrust augmentation, the ITB model outperformed the afterburning model when Thrust Specific Fuel Consumption (TSFC) is compared to increased thrust, but resulted in decreased fan efficiency and High Pressure Compressor (HPC) stall caused by fan overspeed. In the case of Power Extraction (PX) augmentation the ITB engine achieves similar TSFC results without experiencing component efficiency loss or approaching HPC stall. For the PX augmentation model, the pressure drop across the ITB was varied from 4% to 20%. Large pressure drops were found to increase the TSFC and reduce the HPC stall margin for the ITB model. ITBs are expected to achieve pressure drops between 3% and 5% and for this range the ITB will continue to be more fuel efficient than the afterburning engine model.

An experimental investigation was performed focused on integrating the AFIT ITB to accept a common flow source. Three common flow source diffusers with core to bypass inlet area percentage ratios of 80/20, 70/30, and 60/40 were tested. All three diffuser designs were found to suffer from flow reversal in the bypass stream caused by instances of greater total pressure in the core flow than in the bypass flow. The baseline thrust performance for the JetCat P200 Small Turbine Engine (STE), which will serve as the AFIT ITB vitiated air source, was determined and found to be consistent with manufacturer specifications.

15. SUBJECT TERMS

Combustion, Ultra-Compact Combustion, Inter-Turbine Burner, Numerical Propulsion System Simulation

16. SECURITY CLASSIFICATION OF:			17. LIMITATION OF ABSTRACT	18. NUMBER OF PAGES	19a. NAME OF RESPONSIBLE PERSON
a. REPORT	b. ABSTRACT	c. THIS PAGE			Dr. Marc Polanka AFIT/ENY
U	U	U	UU	104	**19b. TELEPHONE NUMBER** *(include area code)* (937) 255-3636 x4714 marc.polanka@afit.edu

Standard Form 298 (Rev. 8–98)
Prescribed by ANSI Std. Z39.18